Scheduling Neural Sensors to Estimate Brain Activity

by

Stefanos Michael

A Thesis Presented in Partial Fulfillment
of the Requirements for the Degree
Master of Science

Approved April 2012 by the
Graduate Supervisory Committee:

Antonia Papandreou-Suppappola, Chair
Chaitali Chakrabarti
Narayan Kovvali

ARIZONA STATE UNIVERSITY

May 2012

ABSTRACT

Research on developing new algorithms to improve information on brain functionality and structure is ongoing. Studying neural activity through dipole source localization with electroencephalography (EEG) and magnetoencephalography (MEG) sensor measurements can lead to diagnosis and treatment of a brain disorder and can also identify the area of the brain from where the disorder has originated. Designing advanced localization algorithms that can adapt to environmental changes is considered a significant shift from manual diagnosis which is based on the knowledge and observation of the doctor, to an adaptive and improved brain disorder diagnosis as these algorithms can track activities that might not be noticed by the human eye. An important consideration of these localization algorithms, however, is to try and minimize the overall power consumption in order to improve the study and treatment of brain disorders.

This thesis considers the problem of estimating dynamic parameters of neural dipole sources while minimizing the system's overall power consumption; this is achieved by minimizing the number of EEG/MEG measurements sensors without a loss in estimation performance accuracy. As the EEG/MEG measurements models are related non-linearity to the dipole source locations and moments, these dynamic parameters can be estimated using sequential Monte Carlo methods such as particle filtering. Due to the large number of sensors required to record EEG/MEG measurements for use in the particle filter, over long period recordings, a large amounts of power is required for storage and transmission. In order to reduce the overall power consumption, two methods are proposed. The first method used the predicted mean square estimation error as the performance metric under the constraint of a maximum power consumption. The performance metric of the second method uses the distance between the location of the sensors and the location estimate of the dipole source at the previous time step; this sensor scheduling scheme results in maximizing the overall signal-to-noise ratio. The performance of both methods is demonstrated using simulated data, and both methods show that they can provide good estimation results with significant reduction in the number of activated sensors at each time step.

ACKNOWLEDGEMENTS

First and foremost I am heartily thankful to my advisor, Dr. Antonia Papandreou-Suppappola, for giving me the opportunity to work as one of her students and for providing me constant assistance and advice. It was a pleasure working with her and her academic experience and passion for the field of statistical signal processing have been valuable guidance to me. I am particularly grateful for her patience, her kindness and her support throughout my thesis. She was like a second family to me and this thesis would not have been possible without her.

In addition, I would like to thank Dr. Chaitali Chackrabarti and Dr. Narayan Kovvali for their willingness and interest to be part of my thesis committee. Their comments and suggestions were significantly helpful to me. I would like to further thank Dr. Narayan Kovvali for helping me understand the sensor scheduling optimization problem.

Furthermore, I am grateful to my colleague and very good friend Lifeng Miao, who was my mentor from the very beginning of my research. Lifeng was the one that introduced me to the neuron activity model and helped me learn how to implement the particle filter algorithm. The fact that we were both a part of the same project was of great importance to me, since it helped me overcome a lot of difficulties.

Moreover, I would like to thank all my colleagues in the lab; Meng Zhou, Shubo Liu, Brian ODonnell, Karl Dutson for their help in MATLAB programming and other aspects of the project.

Finally, I would like to thank my family for always being there for me. With their constant support and motivation I was able to successfully complete my Master studies.

TABLE OF CONTENTS

LIST OF TABLES

LIST OF FIGURES

List of Symbols

C_m	Power consumption of the mth sensor	26
SNR	Signal-to-noise ratio	28
$\mathfrak{s}$	Number of sensors that are picked to be activated per dipole	29

Chapter 1

INTRODUCTION

1.1 Motivation

The brain is the centre of the nervous system of the human body that controls and coordinates the functionality of human muscles. Studying brain disorders that cause abnormal brain functionality has been a topic of ongoing research. One such brain disorder is epilepsy, a condition characterized by transient and unexpected electrical disturbances of the brain. The growing rate of people suffering from epilepsy further emphasizes the need for developing advanced processing techniques. Magnetoencephalography (MEG) and electroencephalography (EEG) are test techniques that record the electrical and magnetic brain activity due to electrode sensors placed along the scalp. EEG/MEG methods directly measure electrical brain activity and provide high time resolution, which provides the ability to obtain information on the dynamic characteristics of the brain function. This is an advantage of the EEG/MEG method over other methods, such as functional magnetic resonance imaging (fMRI), which provide higher spatial resolution than the EEG/MEG methods [3]. The location resolution drawback of the EEG/MEG methods, however, can be solved by solving the electromagnetic inverse problem. By using the measurements of multiple sensors (electrodes) that are attached on the human skull and by solving the inverse problem using signal processing methods, the results can be used to predict and identify brain disorders, such as epilepsy.

A new technique known as ambulatory EEG (AEEG) is used nowadays that improves the quality and accuracy of brain disorder tests. According to this method, the EEG system is portable and can be used in the natural environment of the patient, which could be, for example, the cause the seizure disorder. The disadvantage of the current AEEG is the inconvenience caused to the patient due to the application of electrode's wires and the high weight of the system. To overcome the disadvantages of the current AEEG, a new method called wearable EEG is proposed in order to replace the heavy and inconvenient AEEG. The proposed devices are smaller and are easily attached on the scalp of the patient and can record EEG for longer periods [4–6]. The proposed method will be an evolution in the field of brain disorders monitoring. It will provide long term monitoring of brain activ-

ity, which is important for some brain disorders, and can help identify a higher likelihood of seizures.

There are several issues that researchers need to overcome in order to make AEEG a reliable and beneficial device for studying brain disorders. The first issue is to ensure that the electrodes stay attached on the patient's head. Since this is a device that can be wearable in the patient's nature environment, it is possible for one or more of the electrodes to detach from the scalp due to the movements of the patient. If one electrode is detached during testing, then bad measurements are obtained and the test is not reliable for study. The second constraint is the weight of the device. It has to be light in order to be convenient. The third constraint is to minimize the wire connections. Each channel requires a single wire to connect the electrode to the recorded device. The new device has to be convenient and should not restrict the movement range of the patient. The fourth constraint of the new device is the ability to store and transmit a large amounts of data that long period recordings require [4]. According to [4], for a 24 hour period recording, approximately 1GB of memory is required. This raises a power constrain issue, since in order to achieve long term recordings, a large amount of power is needed. Finally, the last constraint is the time required by the neurologist to analyse the data [7].

This thesis research focuses on the high power consumption constraint because of the long term data recording requirement. The necessity and importance of monitoring brain disorders makes it necessary to investigate various methods in order to overcome the power constraint obstacle. Some existing proposed methods are: data selection techniques [8], data compression techniques [9] and wavelet methods [10]. In addition, a group of researches attempted to reduce the power constraint by hardware improvement, such as amplifier design [6]. We propose to reduce the total power consumption by reducing the number of activated sensors at each time step using sensor scheduling.

1.2 Neuron activity tracking

Over the last years, neuron source localization using EEG/MEG measurements drew the attention of many researchers and a lot of algorithms have been developed to provide more efficient results in brain disorders diagnosis. Designing advanced localization algorithms

that can adapt to environmental changes is considered a significant shift from manual diagnosis which is based on the knowledge and observation of the doctor, to an adaptive and improved brain disorder diagnosis as these algorithms can track activities that might not be noticed by the human eye. An important consideration of these localization algorithms, however, is to try and minimize the overall power consumption in order to improve the study and treatment of brain disorders [11–13]. Based on the nonlinear relationship between EEG/MEG measurements and dipole source parameters at different time steps, sequential Monte Carlo techniques like particle filtering can be used to estimate the time-varying dipole source parameters. These techniques have the advantage of improving neuron estimation performance and can also be applied to hardware implementation [11, 12].

1.3 Sensor Scheduling

Although particle filtering can be used for estimating dipole source parameters, it has high computational cost, which is a disadvantage, and also requires a large amount of data to be analysed. We propose a sensor scheduling algorithm which identifies a subset of sensors to be powered on, thereby significantly reducing the power consumption of the EEG system. The algorithm is based on adaptively configuring the sensors used to collect the EEG measurements at each time step using the minimum predicted mean-squared error or maximum signal-to-noise ratio (SNR) as the performance metric. Optimization is performed globally over the entire search space of all available sensors. We show that the proposed sensor scheduling algorithm significantly reduced the number of sensors required with minor loss in estimation performance degradation. Optimizing a sensor scheduling algorithm can provide good estimation results with a smaller amounts of data. Using sensor scheduling for radar tracking shows that choosing the optimum sensor combination can provide good estimation results [14, 15]. Therefore, sensor scheduling can be used to optimize the sensor combination that provides the most valuable information for dipole locations. In addition, the use of fewer sensors can reduce false alarms or artifacts, which constitute noise coming from either brain activities related to body muscles that are not valuable in the brain study or hardware noise.

In this thesis, two methods of sensor scheduling are introduced. Both of them use

the particle filter as the state estimate filtering tracking technique, because of the advantage that it can be used in non-linear and non-Gaussian dynamic models. The first method uses the predicted root mean-squared error (RMSE) as a performance metric for optimizing the sensor configuration. The second method, which is a heuristic method, uses the distance between the sensor location and the dipole location at the previous time step.

1.4 Thesis Organization

This thesis is organized as follows. Chapter 2 provides background information on the modelling of EEG/MEG measurements and then introduces the forward problem with the inverse solution.

In Chapter 3, Bayesian estimation is discussed based on the state space formulation of the problem. Because the forward problem is a non-linear problem with respect to the location of the dipole, the particle filtering algorithm is used. As a result, the particle filter algorithm is discussed with examples of previous tracking simulations on multiple dipole tracking.

In Chapter 4, the two sensor scheduling methods are discussed in detail. For each technique, the method is explained in detail with diagrams. In Chapter 5, all the simulations and results are discussed. A number of tables and three-dimensional (3-D) plots are used that demonstrate the performance of each method.

Chapter 2

NEURAL ACTIVITY DIPOLE SOURCE MODEL

This section is going to introduce to the reader the physics background on the MEG/EEG source localization problem. The first step in solving this problem is to calculate the potential and magnetic fields of the primary currents based on the neural activity; this is known as the forward problem. In reality, the primary current source is not a discrete element and, as a result, the dipole source approximation is needed before the forward problem is considered. Based on the forward model, the primary current location can be estimated using the inverse problem. The dipole source model for both EEG and MEG measurements is first provided, before a brief introduction of the most known sensor placement systems is discussed. We also provide a short discussion on MEG/EEG artifacts. The presence of artifacts is an important aspect that needs to be addressed in order to obtain more accurate results when estimating neural activity.

2.1 Dipole Representation and Current Distribution

The brain has a lot of neural current sources that can cause scalp potentials and external magnetic fields. Those neural activities can be measured using MEG/EEG methods. However, it is important to distinguish the signals that are important in the specific research problem or brain disorder diagnosis. These signals can be separated in the primary currents $\mathbf{I}^p$, also known as microscopic currents, as well as in the secondary currents, also known as volume currents $\mathbf{I}^v$. The primary currents are microscopic cellular currents, which contain valuable information on neural activity. On the other hand, the volume currents represent the movement charge of surrounding tissue caused by macroscopic electric fields [16]. Volume currents can be considered as noise; they are also known as EEG/MEG artifacts. Thus, the currents at each three-dimensional (3-D) observation point $\mathbf{r}$ can be expressed as

$$\mathbf{I}(\mathbf{r}) = \mathbf{I}^p(\mathbf{r}) + \mathbf{I}^v(\mathbf{r}) \tag{2.1}$$

The primary current is the only current component that is used in the calculation of the potentials and magnetic fields of brain activity. In order to make a model of this primary current in terms of source localization, it is assumed that the primary current acts as a discrete current dipole. This is a very useful and accurate estimation because the dipole

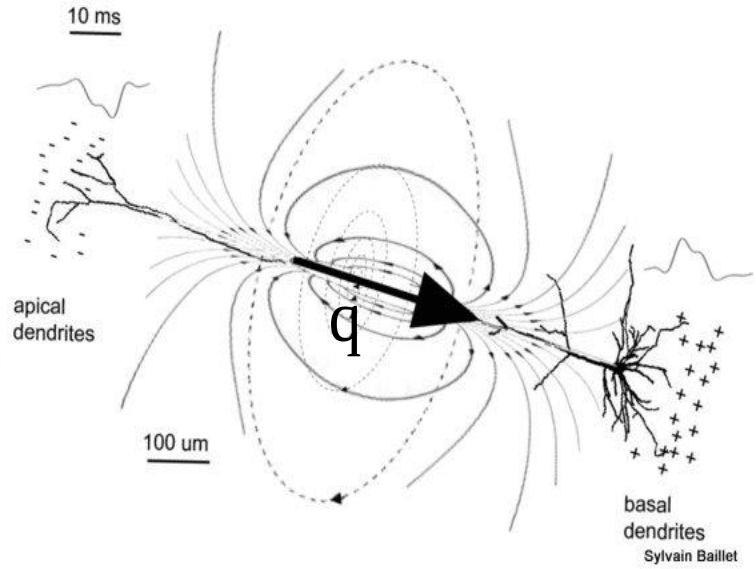

Figure 2.1: A small scale picture representation of the ionic current activity of a large neural cell and the arrow indicates the dipole estimation with moment $\mathbf{q}$ [1]

represents the motion of a local charge over a small distance. The direction of the dipole is the same as the primary current $\mathbf{I}^p(\mathbf{r})$ and multiplying current with distance gives the moment $\mathbf{q}$ of the current dipole. Therefore, the primary current $\mathbf{I}^p(\mathbf{r})$ can be discretized at a single point as a current dipole with moment $\mathbf{q}_j$ at location $\mathbf{r}_j$ [16]. The primary current discretization can also be shown mathematically as a delta function. Therefore, the primary current $\mathbf{I}^p_k$ at time k can be represented in terms of N_d current dipoles as

$$\mathbf{I}^p_k(\mathbf{r}) = \sum_{j=1}^{N_d} \mathbf{q}_{k,j}\delta(\mathbf{r}-\mathbf{r}_{k,j}) \tag{2.2}$$

where $\mathbf{q}_k = [q_k^{(x)}\ q_k^{(y)}\ q_k^{(z)}]$ and $\mathbf{r}_k = [r_k^{(x)}\ r_k^{(y)}\ r_k^{(z)}]$ are 3-D moment and location vectors, respectively, in Cartesian coordinates for the jth dipole at time step k. Equation (2.2) is very important and will be used in the next section in order to define the forward problem. Figure 2.1 and Figure 2.2 show how the dipole approximation actually looks in the brain structure. Figure 2.1 shows how the neuron cells are polarized causing the current to flow through them, indicating the current dipole approximation. Figure 2.2 shows in large scale

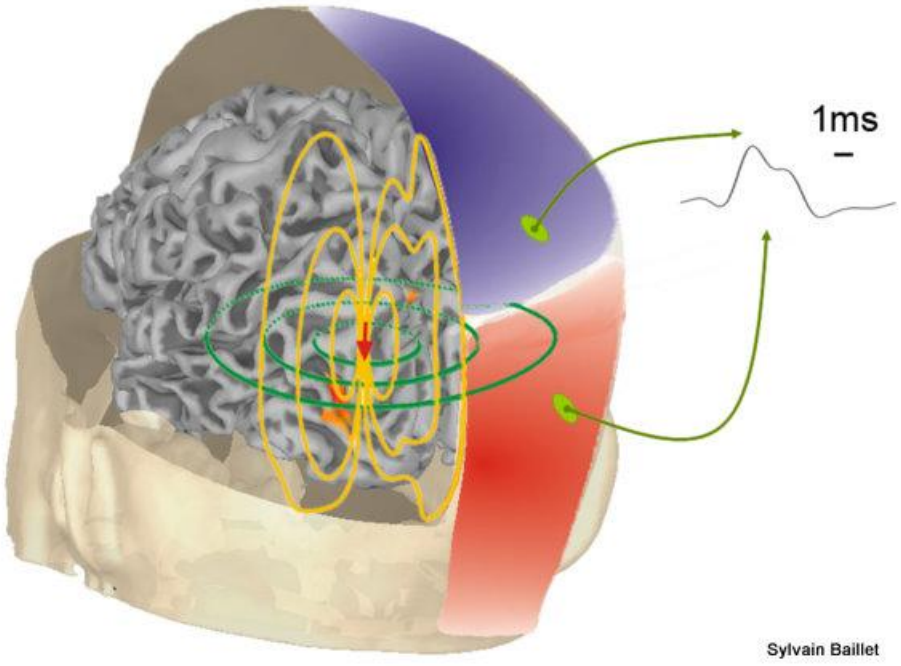

Figure 2.2: A large scale picture indicating the effects of current movement with the arrow indicating the dipole representation [1]

the dipole formation according to the current movement. The arrow in both figures indicates the dipole approximation and direction.

2.2 The Forward Model

The current dipole with moment $\mathbf{q}_j$ at location $\mathbf{r}_j$ is related to the surface potential $u(\mathbf{r})$ at location $\mathbf{r}$ using the forward model [16, 17]. The formulation and solution of the problem is based on Maxwell's equations and the quasi-static approximation of Maxwell's equations [16]. Because of the nature of EEG/MEG signals, the time derivatives are really small and, according to the quasi-static approximation, these can be ignored. The head model is another important factor in defining the forward problem. In order to calculate the magnetic fields, it is important to know the conductivity σ of the head volume and in how many regions the head is divided. Most of the head models divide the human head from one to five regions, also known as shells (scalp, skull, cerebrospinal fluid, gray matter and white matter), where the conductivity $\sigma(\mathbf{r})$ is assumed to be uniform in each region [18, 19]. Applying the quasi static approximation and the head model, the electric field can be

described as [16, 17]

$$\mathbf{b(r)} = \mathbf{b}_\infty(\mathbf{r}) - \frac{\mu_0}{4\pi}\sum_{i=1}^{\psi}(\sigma_i^- - \sigma_i^+)\int_{S_i}(u(\mathbf{r'})n_i(\mathbf{r'}) \times \frac{\mathbf{d}}{d^3})d\mathbf{r'} \tag{2.3}$$

where $(\mathbf{a} \times \mathbf{b})$ denotes the cross product between vectors $\mathbf{a}$ and $\mathbf{b}$, $\mathbf{d} = \mathbf{r} - \mathbf{r'}$ is the distance between the observation point $\mathbf{r}$ and the source point $\mathbf{r'}$ with magnitude d, S_i is the number of surfaces between the uniform regions, and each surface has an inside and outside σ_i^- and σ_i^+ respectively. The number of regions is always $\Psi + 1$, because it includes the non-conductive region outside the head. Therefore, the number of surfaces S_i that are between the regions is always greater than the number of regions, $\psi \geq \Psi$. $\mathbf{n}_i(\mathbf{r})$ is a vector element of S_i. The primary field $\mathbf{b}_\infty(\mathbf{r})$ is defined as [17]

$$\mathbf{b}_\infty(\mathbf{r}) = \frac{\mu_0}{4\pi}\int_C \mathbf{j}^p(\mathbf{r}') \times \frac{\mathbf{d}}{d^3}d\mathbf{r'} \tag{2.4}$$

where μ_0 is permittivity of free space and $\mathbf{j}^p$ is the primary current. Applying Green's theorem, the surface potential at all surfaces can be calculated using

$$\sigma_0 u_\infty(\mathbf{r}) = \frac{(\sigma_i^- - \sigma_i^+)}{2}u(\mathbf{r}) + \frac{1}{4\pi}\sum_{i=1}^{\psi}(\sigma_i^- - \sigma_i^+)\int_{S_i}(u(\mathbf{r'})n_i(\mathbf{r'}) \times \frac{\mathbf{d}}{d^3})d\mathbf{r'} \tag{2.5}$$

where $\mathbf{r} \in S_i$, and $u_\infty(\mathbf{r})$ is the primary potential defined as

$$u_\infty(\mathbf{r}) = \frac{1}{4\pi\sigma_0}\int_G \mathbf{j}^p(\mathbf{r'}).\frac{\mathbf{d}}{d^3}d\mathbf{r'} \tag{2.6}$$

Based on the current dipole approximation, Equations (2.4) and (2.6) of the primary field and primary potential can be simplified to

$$\mathbf{b}_\infty(\mathbf{r}) = \frac{\mu_0}{4\pi}\mathbf{q} \times \frac{\mathbf{d}}{d^3}d\mathbf{r'} \tag{2.7}$$

$$u_\infty(\mathbf{r}) = \frac{1}{4\pi\sigma_0}\mathbf{q}.\frac{\mathbf{d}}{d^3}d\mathbf{r'} \tag{2.8}$$

At this point, it is important to define the forward problem based on the location $\mathbf{r}_m$ of the mth sensor and the MEG symmetric conductor, which is the head. Therefore, the radial field component for each sensor location $\mathbf{r}_m$ with magnitude r can be defined as [16]

$$\begin{aligned} b_r(\mathbf{r}_m) &= b_\infty(\mathbf{r}_m) \cdot \frac{\mathbf{r}_m}{r} \\ &= \frac{\mu_0}{4\pi}\mathbf{r}_m \times \mathbf{r}_j \cdot \frac{\mathbf{q}_j}{rd^3} \end{aligned} \tag{2.9}$$

The radial magnetic field is important because it is used to calculate the magnetic potential $u(\mathbf{r}_m)$. Calculating the magnetic potential $u(\mathbf{r}_m)$, the full magnetic field can be finally obtained in Cartesian coordinates by taking the gradient of $u(\mathbf{r}_m)$ using Sarvas's formula [16]. The full magnetic field is basically the forward problem of MEG. Specifically, the full magnetic field $b_{k,j}(\mathbf{r}_m)$ for the mth sensor, with position $\mathbf{r}_m$ at time step k for the jth dipole is given by

$$b_{k,j}(\mathbf{r}_m) = \left[\frac{\mu_0}{4\pi g^2(\mathbf{r}_{k,j},\mathbf{r}_m)}\,\mathbf{r}_{k,j}\times\Big(g(\mathbf{r}_{k,j},\mathbf{r}_m)\,\mathbf{q}_m - \mathbf{f}^T(\mathbf{r}_{k,j},\mathbf{r}_m)\mathbf{q}_m\,\mathbf{r}_m\Big)\right]^T \mathbf{q}_{k,j} \tag{2.10}$$

The scalar $g(\mathbf{r}_{k,j},\mathbf{r}_m)$ and the vector $\mathbf{f}(\mathbf{r}_{k,j},\mathbf{r}_m)$ are obtained as

$$g(\mathbf{r}_{k,j},\mathbf{r}_m) = d_{k,m,j}\left(d_{k,m,j}\,|\mathbf{r}_m| + |\mathbf{r}_m|^2 - \mathbf{r}_{k,j}^T\mathbf{r}_m\right) \tag{2.11}$$

$$\begin{aligned}\mathbf{f}(\mathbf{r}_{k,j},\mathbf{r}_m) = &\left(\frac{d_{k,m,j}^2}{|\mathbf{r}_m|} + \eta_{k,m,j} + 2\,d_{k,m,j} + 2\,|\mathbf{r}_m|\right)\mathbf{r}_m \\ &- \Big(d_{k,m,j} + 2|\mathbf{r}_m| + \eta_{k,m,j}\Big)\,\mathbf{r}_{k,j}\end{aligned} \tag{2.12}$$

where $\eta_{k,m,j} = (\mathbf{r}_{k,j} - \mathbf{r}_m)^T\mathbf{r}_m/d_{k,m,j}$, μ_0 is the permittivity of free space, and $d_{k,m,j}$ is the distance between the jth dipole source and the mth sensor. For the EEG, a similar equation can be formed for the case of a single shell model, where the conductivity of the head is assumed to be uniform over all the volume of the head. The potential then is given by [16]

$$\begin{aligned}u(\mathbf{r}_m;\mathbf{r}_{k,j},\mathbf{q}) = &\frac{1}{4\pi\sigma}\cos(\alpha_{k,j}) \\ &\left[\frac{2}{d_{k,m,j}^3}\Big(|\mathbf{r}_{k,j}|\cos(\gamma_{k,m,j}) - r\Big) + \big(d_{k,m,j}\,|\mathbf{r}_{k,j}|\big)^{-1} - \big(r\,|\mathbf{r}_{k,j}|\big)^{-1}\right] \\ &+ \frac{1}{4\pi\sigma}\sin(\alpha_{k,j})\cos(\beta_{k,j})\sin(\gamma_{k,m,j}) \\ &\left[\frac{2\,r}{d_{k,m,j}^3} + \frac{d_{k,m,j} + r}{r\,d_{k,m,j}\,(r - |\mathbf{r}_{k,j}| + d_{k,m,j})}\right]\end{aligned}$$

where r is the radius of the head model, $\gamma_{k,m,j}$ is the angle between the vector pointing to the mth sensor and the vector pointing to the jth dipole location, $\alpha_{k,j}$ is the angle between the jth dipole orientation and the vector pointing to the jth dipole location, $\beta_{k,j}$ is the angle between the plane formed by the jth dipole and the origin. Also, $|\mathbf{r}_{k,j}| = \big[(r_{k,j}^{(x)})^2 + (r_{k,j}^{(y)})^2 + (r_{k,j}^{(z)})^2\big]^{1/2}$ in (2.13).

2.3 The Inverse Problem

The inverse problem is the estimation of the position and moments of the dipole sources. As mentioned above, the inverse problem is the issue of localizing the state of dipoles. Based on the forward model in the previous section, the measurements are linear with respect to the moment $\mathbf{q}_k$ and non-linear with respect to the dipole location $\mathbf{r}_{k,j}$ [16, 17]. By separating the moment parameters $\mathbf{q}_k$ from the non-linear location parameters $\mathbf{r}_{k,j}$, it becomes less complicated to solve the inverse problem [16]. Therefore, the magnetic field Equation (2.10) can be written as the inner product of the lead field vector $g(\mathbf{r}_m, \mathbf{r}_{k,j})$ and the dipole moment $\mathbf{q}_k$. In the MEG case with m number of sensors, the magnetic field can be expressed as

$$\begin{bmatrix} b_{k,j}(\mathbf{r}_1) \\ \dots \\ b_{k,j}(\mathbf{r}_{N_s}) \end{bmatrix} = \begin{bmatrix} g(\mathbf{r}_1, \mathbf{r}_{k,j})^T \\ \dots \\ g(\mathbf{r}_{N_s}, \mathbf{r}_{k,j})^T \end{bmatrix} \mathbf{q}_k \tag{2.13}$$

The same formation can be developed in the EEG case with the only difference that, instead of using the magnetic field, the potential of Equation (2.13) is used. The leadfield matrix, also known as 'gain matrix', correlates the set of discrete sensor locations $\mathbf{r}_m$ to the dipole at $\mathbf{r}_{k,j}$ [17]. The leadfield matrix for the MEG measurements is Equation (2.10) and for the EEG, it is Equation (2.13). Therefore, considering N_d dipole sources and N_s MEG/EEG measurements sensors over K time steps, the forward model can be expressed by [17]

$$\mathbf{F} = \mathbf{G}\mathbf{Q} + \mathbf{W} \tag{2.14}$$

where the $N_s \times K$ matrix $\mathbf{F}$ represents the field measurements of the sensors, the $N_s \times 3N_d$ matrix $\mathbf{G}$ is the gain matrix of the leadfield (where $3N_d$ represents the 3-D moments of N_d dipoles), $\mathbf{Q}$ is a $3N_d \times K$ matrix, that represents the moments of dipoles, and the $N_s \times K$ matrix $\mathbf{W}$ represents the measurement noise. Equation (2.14) is significant in order to optimize the problem and can be used in the particle filter algorithm as the measurement equation when estimating the source location.

2.4 EEG/MEG Artifacts

EEG artifacts are characterized as false alarm signals in the EEG/MEG data. The source of artifacts can be very unexpected. The reason of that is the multiple sources that may cause unwanted signals. Artifacts can be divided into two main categories, the external and internal artifacts.

The external artifacts are mainly caused by the hardware. They can be any noise coming from the electrodes or from any other hardware in use. They can also be caused by magnetic fields of other devices close to the EEG hardware. In addition, if an electrode is not attached properly on the patient's head, this will result in a failure to record the right potential of brain activity.

On the other hand, internal arifacts are caused by activities produced from movements of the patient. The volume current discussed in the previous section is actually an example of internal artifacts. There are a lot of muscles that can cause electric potential, which can be picked up by the electrodes. The most important of those are the ocular artifacts, the myogenic artifacts and the cardiogenic arttifacts. Ocular artifacts are caused by the movement of the eyes. Specifically, a movement of the eyelids or eyeballs results in a change in the electrical field that is recorded by the electrodes. The signal characteristics of ocular artifacts are standard, which makes it easier to identify them [20]. Myogenic artifacts are the different muscle potentials on the scalp that can be caused by the jaw and various movements of the face. The last main category is the cardiogenic artifacts, which are produced by the heart activity. A pulse of the heart produces an electric potential that is noticeable on the scalp. Usually, those artifacts are more noticeable if the electrode is close to a pulsating vessel. As a result, each time the heart produces a pulse, the electrode moves.

The main method used today to decompose the MEG/EEG signal from the artifacts is the independent component analysis (ICA) integrated with time-frequency techniques [21–23]. After the decomposition of the data based on the artifacts' properties, the dipole signal can be identified. This is another big area of research in which many papers have been published.

2.5 Electrode Systems

The aim of this thesis is to optimize the sensor configurations that need to be activated at each time step. Therefore, it is important to introduce the sensor systems that are used for the sensor placement and the sensor net structure. The sensor placement on a patient's scalp is really significant in order to obtain good measurements. A lot of electrode systems are proposed, but we discussed two of the most well known ones. The first one is the international standard system for electrode placement, which is also known as the 10-20 system [24,25]. This system was first introduced by Jasper in 1958 [26], and it has been applied in the EEG ever since. The 10-20 system describes the locations that electrodes need to be placed. These locations are calculated based on relative distances between cranial landmarks over the head surface [24,25]. Even though this is the international standard, the study of new methods for the signal source localization resulted in the development of other systems, such as the 10-10 or 10-5, which basically increase the electrodes' density [24]. Figure 2.3 shows the 10-20 system, where A=ear lobe, Pg=nanopharyngeal, P= pariental, F=frontal, Fp=frontal polar, and O=occipital [2].

Most of the current EEG tests use the EEG geodesic sensor net, which was first proposed in 1993 [25]. The geodesic sensor net organizes and fixes the sensor on a 2-D array. Sensors are fixed at each geodesic vertex, which insures that the arrays are evenly distributed across the head surface [25]. The term geodesic is an approximation of a curve using a straight line and is usually used for sphere shape approximations. Figure 2.4 indicates how the human head is divided in different geodesic vertexes, indicating where the electrodes need to be placed [25]. The particular example is for a 128 channel geodesic sensor net. The position of each sensor is important to be specified accurately, because a wrong placement will result in wrong electrical measurements, since electrical measurements are related to brain anatomy.

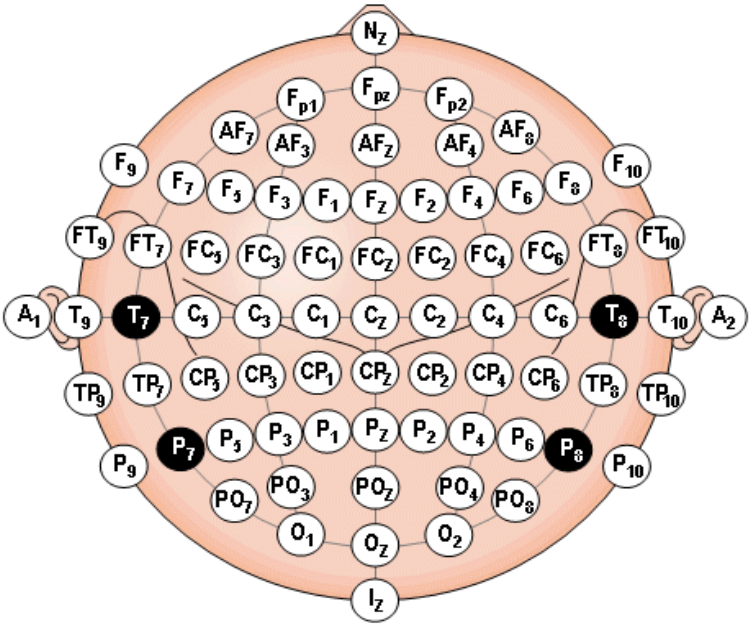

Figure 2.3: International 10-20 system diagram describing the location that each electrode need to be placed on patient's scalp; diagram taken from [2].

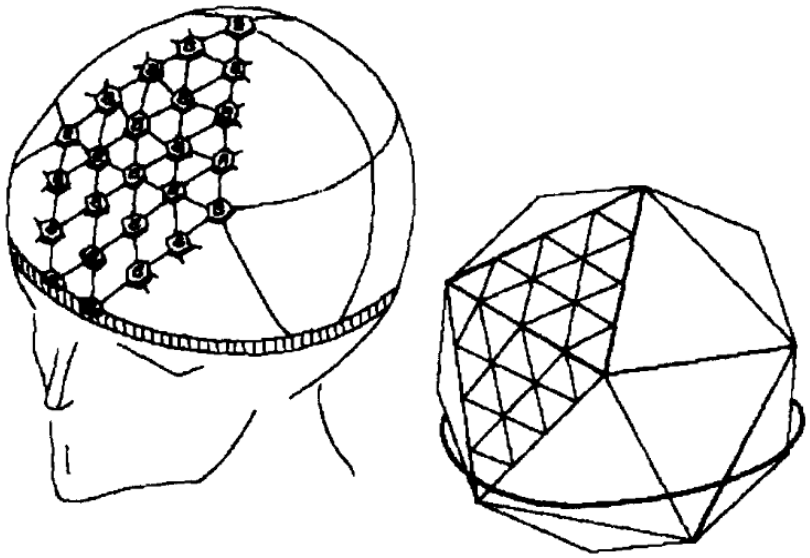

Figure 2.4: Geodesic sensor net structure for 128-channel demonstrating the geodesic vertexes that each sensors need to be placed; diagram taken from [2].

Chapter 3

DIPOLE SOURCE PARAMETER ESTIMATION USING PARTICLE FILTERING

Neural activity information can be obtained by estimating the location and moment of dipole sources using MEG/EEG sensor measurements. As the parameters to be estimated change with time are non-linearly related to the measurements, particle filtering can be used for the estimation.

In this section, the state-space formation is first introduced. Subsequently, a review of Bayesian theory is also presented in order to recursively estimate the dipole source unknown parameters. Furthermore, the particle filtering algorithm is discussed and, finally, a particle filter (PF) example on a multi-dipole case is presented .

3.1 Recursive Bayesian Estimation

Recursive Bayesian estimation is a process that recursively estimates the an unknown source parameter or state $\mathbf{x}_k$ of a dynamic system, where $\mathbf{x}_k \in \mathbb{R}^{n_x}$, from a noisy measurement $\mathbf{y}_k \in \mathbb{R}^{n_x}$, and $\mathbb{R}$ represents all the real numbers and $k \in \mathbb{N}$ [27, 28]. The state at the current time step is related to its value at the previous time step according to the state equation given by

$$\mathbf{x}_k = \mathbf{f}_{k-1}(\mathbf{x}_{k-1}, \mathbf{v}_{k-1}) \tag{3.1}$$

Equation (3.1) shows that it is calculated based on the (possibly) non-linear function $\mathbf{f}_{k-1}(\mathbf{x}_{k-1})$, which is written as a function of the prior state $\mathbf{x}_{k-1}$ and the modelling error process $\mathbf{v}_{k-1}$. For example, in a radar application, the state equation can be a vector representation of the velocity, the acceleration and the position of a moving target. In this specific case, the state space is the position and the moment of the dipole and is a six dimensional vector. The measurement equation is given by

$$\mathbf{y}_k = \mathbf{h}_k(\mathbf{x}_k, \mathbf{w}_k) \tag{3.2}$$

and it describes the measurement $\mathbf{y}_k$ as a function of the state $\mathbf{x}_k$ using the possibly non-linear function $\mathbf{h}_k(\mathbf{x}_k)$. As observed in Equation (3.2), $\mathbf{y}_k$ is written as a function of the target state $\mathbf{x}_k$ and $\mathbf{w}_k$ is the measurement noise vector.

In order to solve the estimation problem of the state equation based on the measurement equation, the Bayes' theorem is applied. According to Bayes' theorem, the conditional distribution $p(\mathbf{x}_k|\mathbf{Y}_{1:k})$ represents the posterior information of $\mathbf{x}_k$ given $\mathbf{Y}_{1:k}$, where $\mathbf{Y}_{1:k} = [\mathbf{y}_1^{\mathrm{T}}\ \mathbf{y}_2^{\mathrm{T}}\ ...\ \mathbf{y}_k^{\mathrm{T}}]^{\mathrm{T}}$ [27]. Using the Bayes' theorem formula given by

$$p(\mathbf{x}_k|\mathbf{Y}_{1:k}) = \frac{p(\mathbf{y}_k|\mathbf{x}_k)p(\mathbf{x}_k|\mathbf{Y}_{1:k-1})}{p(\mathbf{y}_k|\mathbf{Y}_{1:k-1})} \tag{3.3}$$

where the denominator of Bayes' theorem is given by

$$p(\mathbf{y}_k|\mathbf{Y}_{1:k-1}) = \int p(\mathbf{y}_k|\mathbf{x}_k)p(\mathbf{x}_k|\mathbf{Y}_{1:k-1})d\mathbf{x}_k \tag{3.4}$$

where the probability distribution $p(\mathbf{x}_k)$ models the previous knowledge of $\mathbf{x}_k$ and the likelihood density function $p(\mathbf{y}_k|\mathbf{x}_k)$ models the relationship between the measurement and state equations.

In order to estimate the most probable state $\mathbf{x}_k$ based on all measurements, the probability density function $p(\mathbf{x}_k|\mathbf{Y}_{1:k})$ needs to be constructed. The construction process can be divided in two stages: the prediction and the update stages [27,29]. In order to break the process into these two stages, it is necessary to assume that the previous probability density function $p(\mathbf{x}_{k-1}|\mathbf{Y}_{1:k-1})$ is known. The prediction stage involves the calculation of the probability density function at time k using Equation (3.1) and applying the Chapman-Kolmogorov equation, given by

$$\begin{aligned} p(\mathbf{x}_k|\mathbf{Y}_{1:k-1}) &= \int p(\mathbf{x}_k, \mathbf{x}_{k-1}|\mathbf{Y}_{1:k-1})d\mathbf{x}_{k-1} \\ &= \int p(\mathbf{x}_k, \mathbf{x}_{k-1}, \mathbf{Y}_{1:k-1})p(\mathbf{x}_{k-1}|\mathbf{Y}_{1:k-1})d\mathbf{x}_{k-1} \\ &= \int p(\mathbf{x}_k|\mathbf{x}_{k-1})p(\mathbf{x}_{k-1}|\mathbf{Y}_{1:k-1})d\mathbf{x}_{k-1} \end{aligned} \tag{3.5}$$

Once the probability density function (PDF) at time step k is found, the measurement $\mathbf{y}_k$ can be obtained. Having all this information, the update stage can be built by applying the Bayes' theorem with equations (3.2) and (3.3). Once the PDF $p(\mathbf{x}_k|\mathbf{Y}_{1:k})$ has been computed, the target state estimate can be calculated by applying the minimum mean-squared error (MMSE) given by

$$\hat{\mathbf{x}}_{k|k} = E[\mathbf{x}_k|\mathbf{Y}_k] \triangleq \int \mathbf{x}_k p(\mathbf{x}_k|\mathbf{Y}_{1:k})d\mathbf{x}_k \tag{3.6}$$

where $E[\mathbf{x}_k|\mathbf{Y}_k]$ is the conditional expected value of $\mathbf{x}_k$. In addition, $\hat{\mathbf{x}}_{k|k}$ is the mean of the $p(\mathbf{x}_k|\mathbf{Y}_{1:k})$. Once the new PDF of the current state is estimated using Equation (3.6), the same procedure is repeated for the next time step based on the new state estimate. This process is repeated in order to find an estimated solution, since, in general, this cannot be solved analytically [27]. In order to solve this type of problem, filtering techniques are required according to the nature of the model. Filtering techniques vary based on whether the system is linear and/or Gaussian. In the case of a linear and Gaussian dynamic model, the Kalman filter can be used. In the case of a non-linear and Gaussian model, the extended Kalman filter can be used and in the non-linear, Gaussian or non-Gaussian dynamic model, Particle filters can be used. These are some of the most known and most commonly used Bayesian filtering techniques. The nature of the neural dynamic system makes particle filter the best fit in this thesis. A brief introduction of particle filters follows.

3.2 Particle Filtering

The fact that the particle filter is suitable for the estimation of the state of a non-linear dynamic model with non-Gaussian noise makes it the most suitable Bayesian approach for the state estimate of the dipole source. The idea of particle filtering is to calculate the posterior probability density function $p(\mathbf{x}_k|\mathbf{Y}_{1:k})$ at time k by using a set of N samples (particles), $\{\mathbf{x}_k^i\}_{i=1}^N$, where each particle has a corresponding weight, $\{w_k^i\}_{i=1}^N$. Therefore, the posterior density from the previous sections at k can be approximated as

$$p(\mathbf{x}_k|Y_{1:k}) \approx \sum w_k^i \delta(\mathbf{x}_k - \mathbf{x}_k^i) \tag{3.7}$$

In Equation (3.7), $\mathbf{x}_k$ represents the state at time step k, and $\mathbf{x}_k^i, i = 1,...,N$ are all the support points with corresponding weights $w_k^i, i = 1,...,N$. In addition, all the weights are normalized and, as a result, their sum for each state is one. The particle filtering method belongs to the family of Sequential Monte Carlo methods, which are approximation methods that have been developed and applied in the field of engineering over the last decades. The particle filter, also known as Monte Carlo integration or Sequential Important Sampling (SIS), is widely used in tracking approximation. The Monte Carlo estimation integral is given by

$$I = \int \mathbf{f}(\mathbf{x}) p(\mathbf{x}) dx \tag{3.8}$$

$$I_N = \frac{1}{N}\sum_{i=1}^{N}\mathbf{f}(\mathbf{x}^i) \tag{3.9}$$

where N is the number of samples (particles) and has to satisfy the condition $N \gg 1$ in order to be distributed in line with $p(\mathbf{x})$. Similarly, $p(\mathbf{x})$ is defined as a probability density that satisfies $p(\mathbf{x}) \geq 0$ and $\int p(\mathbf{x})d\mathbf{x} = 1$. According to the law of large numbers, if the samples $\mathbf{x}^i$ are independent, the integral of Equation (3.8) can be written in the form of a summation as shown in Equation (3.9) [27]. Based on this approximation, as the number of particles increases, the particle filter approaches the optimal Bayesian estimate.

As stated above, particle filtering can be applied to a non-linear Bayesian filtering tracking problem. Equations (3.1) and (3.2) describe the state and measurement model equations representing a dynamic system. Particles are composed from an importance distribution and each particle is weighted based on importance weights. This method is also known as importance sampling [27, 29]. To clarify the importance sampling method and the transformation of Equation (3.8) to Equation (3.9), Figure 3.2 demonstrates how the continuous density function can be approximated by a discrete approximation. As it can be seen on the figure the weights are larger on the peaks of $p(\mathbf{x})$, while in the lower values of $p(\mathbf{x})$, the weights are smaller. In other words, the particles that provide good estimates for the state have larger corresponding weights compared to the ones that have bad state estimation. This method is ideal for solving the problem since $p(\mathbf{x}_k|\mathbf{Y}_k)$ cannot be drawn in closed form and, as a result, it cannot be used to draw samples from it. Therefore, $p(\mathbf{x}_k|\mathbf{Y}_k)$ is represented using Monte Carlo particles.

The particle filtering algorithm starts with drawing particles from an important density $q(\mathbf{x}_k|\mathbf{x}^i_{k-1}, \mathbf{Y}_k)$ from the particles $\mathbf{x}^i_{0:k}, i = 1, ..., N$. As shown in Figure 3.2, each particle is characterized with a corresponding weight, which is calculated using

$$w^i_k \propto w^i_{k-1}\frac{p(\mathbf{y}_k|\mathbf{x}^i_k)p(\mathbf{x}^i_k|\mathbf{x}^i_{k-1})}{q(\mathbf{x}^i_k|\mathbf{x}^i_{k-1}, \mathbf{Y}_k)} \tag{3.10}$$

To simplify Equation (3.10), we can choose $q(\mathbf{x}^i_k|\mathbf{x}^i_{k-1}, \mathbf{Y}_k) = p(\mathbf{x}^i_k|\mathbf{x}^i_{k-1})$, and, as a result, the weight equation can be written as

$$w^i_k \propto w^i_{k-1}p(\mathbf{y}_k|\mathbf{x}^i_k) \tag{3.11}$$

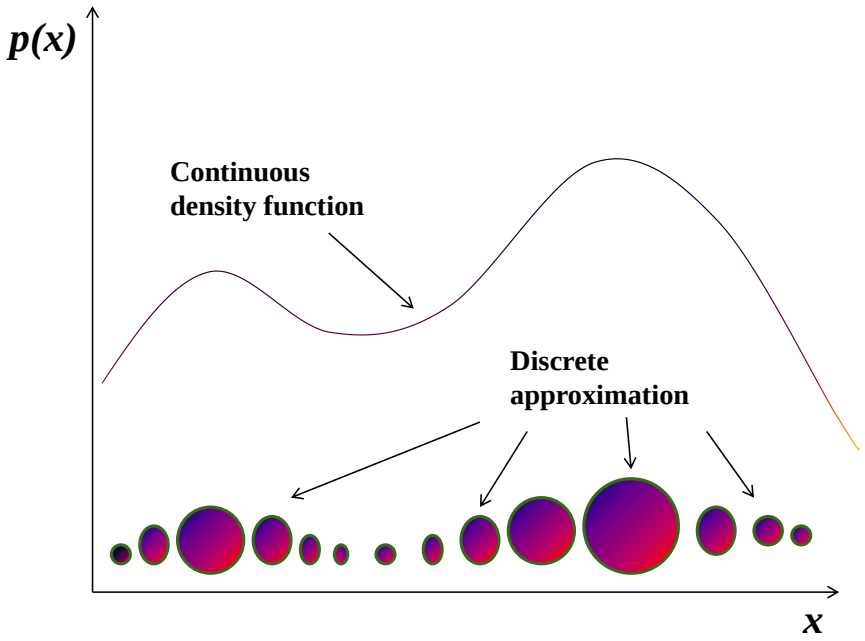

Figure 3.1: An illustration of the importance sampling method. The picture shows the relationship between the continues density function and the discrete approximation, by pointing the importance of weights of the particles.

After the weights are calculated, all the weights are normalized so that their sum for each state equals one. However, the importance weight of a particle sometimes becomes close to zero after a few iterations, which makes it negligible in the calculation process. This problem affects the accuracy of the method, since the weight is concentrated only on a few particles. This problem is known as the degeneracy problem [27]. Using the importance sampling method, the variance increases over time. As a result, the degeneracy problem creates an unavoidable accuracy issue. In order to improve the accuracy of the particle filter when degeneracy occurs, the resampling method is applied. The idea of resampling is to exclude the low importance weights and expand the particles with greater importance weight. Therefore, particles are concentrated where the $p(\mathbf{x}_k|\mathbf{Y}_k)$ is larger. The degeneracy

problem can be solved using the N_{eff}, given by

$$N_{eff} = \frac{1}{\sum_{i=1}^{N} (w_k^i)^2} \tag{3.12}$$

where $1 \leq N_{eff} \leq N$ and w_k^i represents the normalized weight. The larger the N_{eff} is, the smaller the level of degeneracy will be and the other way around. In order to solve degeneracy problem a threshold value N_{thr} is defined. If the $\hat{N}_{eff}$ is smaller than a given threshold N_{thr} , then perform resampling. Table 3.1 provides a summary of the main steps of the particle filter algorithm, including resamlping.

Table 3.1: Particle Filter Sample Algorithm

1. Given $\mathbf{x}_0$, generate N independent particles that provide an estimate of the initial state distribution
2. For each particle:
   - Draw $\mathbf{x}_k^i \sim p(\mathbf{x}_k|\mathbf{x}_{k-1}^i)$
   - Assign a weight for each particle using $w_k^i = w_{k-1}^i p(\mathbf{y}_k|\mathbf{x}_k^i)$
3. Normalize it using $w_k^i = \frac{w_k^i}{\sum_{i=1}^{N}(w_k^i)^2}$
4. Calculate $N_{eff} = \frac{1}{\sum_{i=1}^{N}(w_k^i)^2}$
5. Define a threshold value and do the resampling using $\hat{N}_{eff} < N_{thr}$

3.3 Use of Particle Filtering for Dipole Source Parameter Estimation

In order to use particle filtering to estimate the dipole source parameter, we need to first identify the EEG/MEG dynamic system equations corresponding to (3.1) and (3.2). The measurement equation is by $\mathbf{y}_k = \mathbf{h}(\mathbf{x}_k) + \mathbf{w}_k = \mathbf{G}_k\mathbf{Q}_k + \mathbf{W}_k$. It depends on the lead-field matrix $\mathbf{G}_k$ of EEG and MEG whose elements are respectively given by Equations (2.10) and (2.13). The state equation is assumed of follow a first-order Markov chain model and is given by $\mathbf{x}_k = \mathbf{x}_{k-1} + \mathbf{v}_k$ where $\mathbf{v}_k$ is the modelling process error, $\mathbf{x}_{k-1} = [\mathbf{r}_{k-1,j}\ \mathbf{q}_{k-1,j}]$ is the 3-D moment and location vectors representation in Cartesian coordinates for the jth dipole at time step $k-1$ and $\mathbf{x}_k = [\mathbf{r}_{k,j}\ \mathbf{q}_{k,j}]$ are the unknown state parameters to be estimated for each dipole. We will demonstrate next the use of the particle filter in estimating neural

activity. For this example, all the sensors are used and the main focus is on showing the performance of the particle filter. We evaluate the performance of the estimation, using the root mean-squared error (RMSE). The mean-squared error (MSE) is given by

$$\begin{aligned} \text{MSE}(k) &\triangleq E_{x_k,y_k}[(\mathbf{x}_k - \hat{\mathbf{x}}_k)(\mathbf{x}_k - \hat{\mathbf{x}}_k)^T] \\ &= \int\int (\mathbf{x}_k - \hat{\mathbf{x}}_k)(\mathbf{x}_k - \hat{\mathbf{x}}_k)^T p(\mathbf{y}_k|\mathbf{x}_k) p(\mathbf{x}_k) d\mathbf{x}_k d\mathbf{y}_k \end{aligned} \tag{3.13}$$

By applying the Monte Carlo integration approximation, Equation (3.13) can be written in a summation form as

$$MSE(k) \approx \frac{1}{N}\sum_{i=1}^{N}\frac{1}{M}\sum_{\ell=1}^{M}(\mathbf{x}_k^i - \hat{\mathbf{x}}_k(\mathbf{y}_k^{\ell,i}))(\mathbf{x}_k^i - \hat{\mathbf{x}}_k(\mathbf{y}_k^{\ell,i}))^T \tag{3.14}$$

where $\mathbf{x}_k^i$ are independent and identically distributed (i.i.d) samples drawn from the real state distribution $p(\mathbf{x}_k)$ at time step k, $\mathbf{y}_k^{\ell,i}$ are i.i.d samples drawn using the measurement model (Equation (3.2)), and $\hat{\mathbf{x}}_k(\mathbf{y}_k^{\ell,i})$ is the state estimate using the particle filter algorithm. As previously stated, for the Monte Carlo approximation, as the number of sample increases, the results become more accurate. Therefore, the highest the number of M and N in Equation (3.14), the more accurate the results will be. The RMSE J is the square root of the MSE which it can be calculated by

$$J(k) = \sqrt{MSE(k)} \tag{3.15}$$

In this section, two examples of particle filtering algorithm are introduced to show the effectiveness of the method on the neural source localization problem. The first example is shown in Figure 3.3 and is a tracking study case for 3 dipoles. In this example, probability hypothesis density filtering (PHDF) is used with particle filters in order to track the number of MEG neural dipole sources and their unknown states [11]. The PHDF is used to identify the number of sources and then to recover their location, amplitude and orientation. After the PHDF is applied, the particle filter algorithm is used to estimate the dipole location. In the figure, the continuous line indicates the true dipole location and the circles show the particle filter estimation. From the figure, it can be observed that the particle filter algorithm has a really good performance. The circles are almost in the same path as the true dipole location.

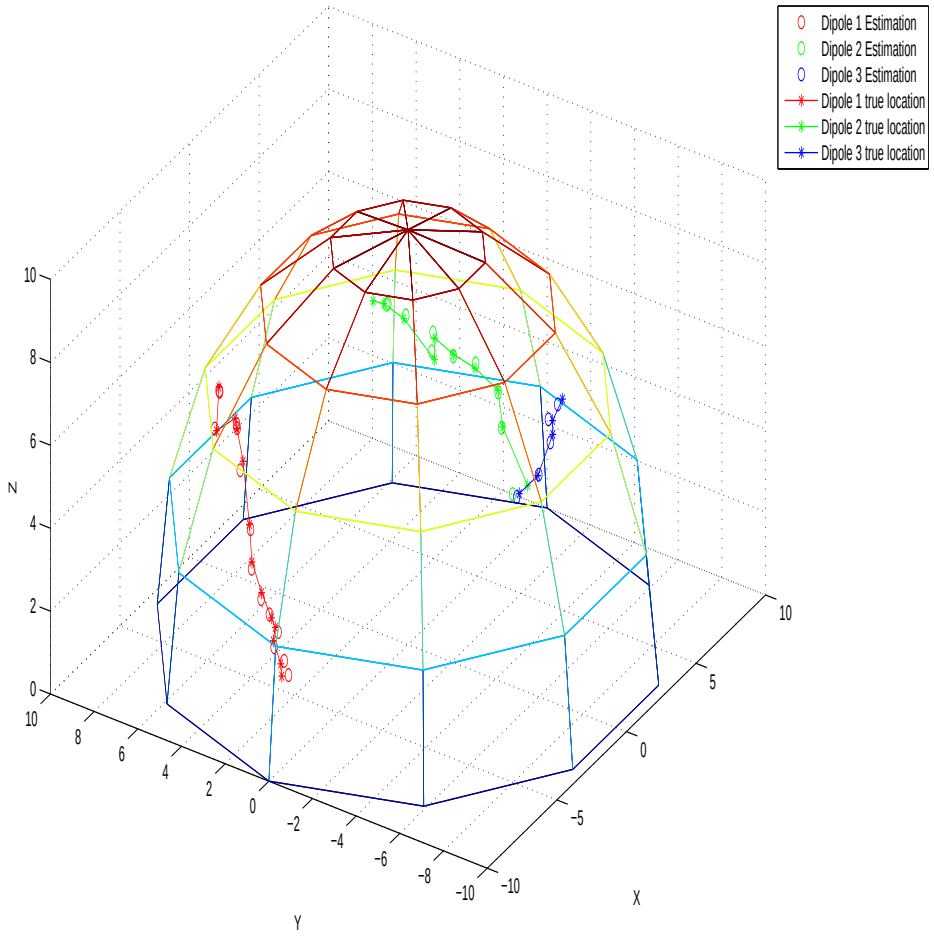

Figure 3.2: 3-Dimensional plot of 3 dipole tracking using particle filter

The second example shows the performance of a particle filter algorithm and a multiple particle filter algorithm in a 2-dipole tracking case [30]. As the number of dipoles increased, the number of dimensions in the state model Equation (3.1) also increased. The multiple particle filter algorithm is usually used when the number of particles is high in order to reduce the complexity of the problem and also reduce the RMSE performance. Therefore, as shown in Figure 3.3, in the case of multiple dipoles, the use of the multiple particle filter algorithm will be more efficient. Both of the methods provide good estimation performance, but the estimation performance of the multiple particle filter is better than the one of the single particle filter.

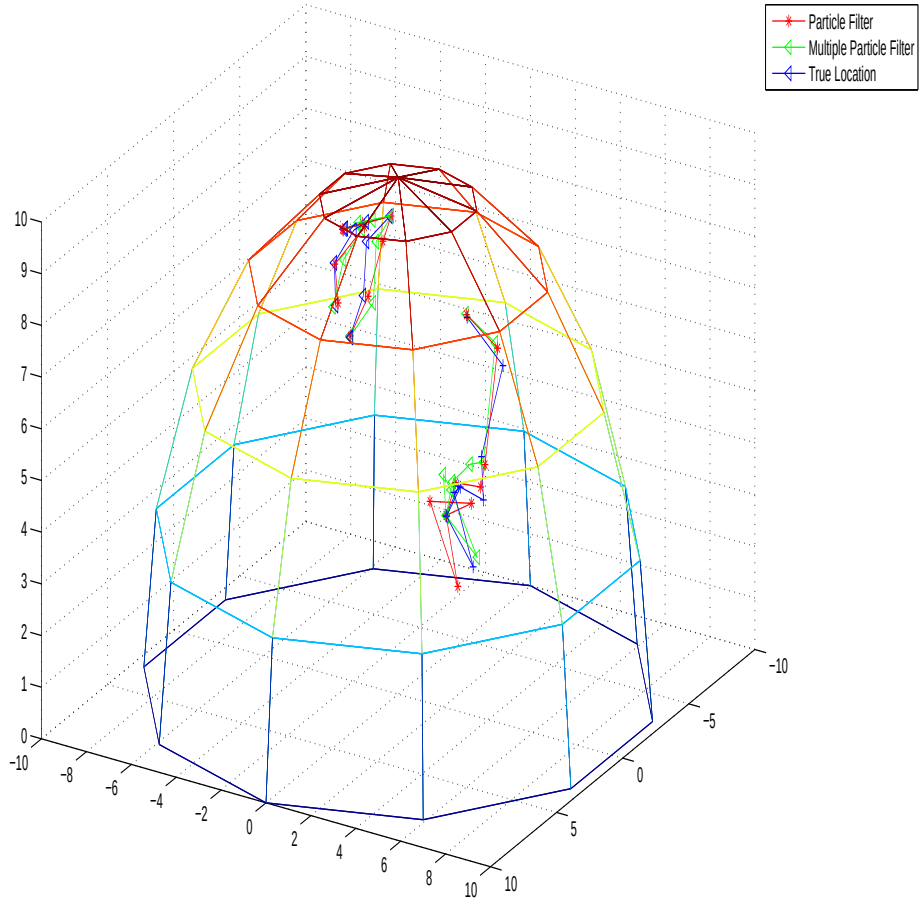

Figure 3.3: 3-Dimensional plot of 2 Dipole tracking using Particle Filter and Multiple Particle Filter

Based on the above examples, it can be concluded that the particle filter algorithm is well-suited for the neural tracking state estimation. Its advantage is that it can be used in a non-linear, Gaussian or non-Gaussian dynamic model, which makes it the best fit in this thesis state estimation problem.

Chapter 4

SENSOR SCHEDULING OPTIMIZATION PROBLEM

Sensor scheduling is a process to allocate sensing resources by optimizing a performance metric over a future time-horizon under constraints. The aim of this work is to reduce the number of sensors while maintaining reasonable estimation performance. As a result, the recorded data for storage and transmission will be reduced, which will also result in reducing the overall power consumption. Therefore, the power constraint of the current AEEG methods will be minimized. The proposed solution of this project is to minimize the number of sensors that are activated at each time step. Reducing the number of sensors will result in minimizing the power consumption of the system. Less sensors means less data for storage and transmission. We propose two different sensor configuration approaches towards solving this problem. The first proposed solution is to adaptively choose the sensor configuration for measurements at each time step that minimize the predicted root mean-squared error (RMSE) as the performance metric. The second proposed solution is a heuristic method that maximizes the SNR, using the distance between the sensor location and the estimated dipole location at the previous time step as the performance metric.

4.1 Sensor Scheduling Using Predicted RMSE

In order to be able to find the optimal sensor configuration using the Bayesian filtering approach, we need to modify the Bayesian problem formulation discussed in Chapter 3. Specifically, we replace the state equation (3.1) and measurement equation (3.2), respectively with

$$\mathbf{x}_k \sim p(\mathbf{x}_k|\mathbf{x}_{k-1}) \tag{4.1}$$

$$\mathbf{y}_k \sim p(\mathbf{y}_k|\mathbf{x}_k, \mathbf{z}_k) \tag{4.2}$$

where $\mathbf{x}_k$ and $\mathbf{y}_k$ are the state and measurement vectors as before. We consider the problem where N_s sensors need to be configured, and we define the sensor configuration vector $\mathbf{z}_k = [z_{k,1}\ z_{k,1}\ \ldots\ z_{k,N_s}]^{\mathrm{T}}$. The sensor configuration vector is comprised of the binary values, $z_{k,m} \in [0,1]$. When $z_{k,m} = 1$, this indicates that the mth sensor is selected. The measurement used at time k depends on this configuration, so the data used is $\mathbf{y}_k(\mathbf{z}_k) = \mathbf{Y}_{k,N_s}$. Based on Equations (4.1) and (4.2), the filtering problem is to estimate the unknown state $\mathbf{x}_k$ based on

k measurements $\mathbf{Y}_k$, which are obtained from k sensor configurations $\mathbf{z}_k$. Assuming that N_s sensors can be used at each time step k, then there are $R = 2^{N_s}$ possible sensor configurations $\mathbf{z}_{k,n}$, $n = 1, \ldots, R$ that can be chosen at time k. A sensor configuration of length N_s is defined as a binary sequence of length N_s that uses the position of a binary digit in the sequence to determine if a sensor is on or off. If the digit is one, then the sensor will be used for measurements; if it is 0, then the sensor will not be used.

The sensor scheduling optimization problem is to find the sensor configuration at each time step that optimizes a cost function under some constraints: (a) that the RMSE only increases by a small amount compared to when all available sensors are used, and (b) the overall power constraint does not exceed a given value. As it is mentioned in Chapter 3, in order to use the Bayesian approach, we begin by assuming that some initial state probability density function $p(\mathbf{x}_0|\mathbf{y}_0, \mathbf{z}_0)$. Then, sequentially, at time step k, the posterior distribution $p(\mathbf{x}_k|\mathbf{Y}_k, \mathbf{Z}_k)$ is computed as

$$p(\mathbf{x}_k|\mathbf{Y}_k, \mathbf{Z}_k) \propto p(\mathbf{y}_k|\mathbf{x}_k, \mathbf{z}_k) \int p(\mathbf{x}_k|\mathbf{x}_{k-1}) p(\mathbf{x}_{k-1}|\mathbf{Y}^{\star}_{k-1}, \mathbf{Z}^{\star}_{k-1}) d\mathbf{x}_{k-1} \tag{4.3}$$

where the star notation indicates the chosen optimum sensor configuration that maximizes the estimation performance for the previous state estimate $\mathbf{x}_{k-1}$. Thus, $p(\mathbf{x}_{k-1}|\mathbf{Y}^{\star}_{k-1}, \mathbf{Z}^{\star}_{k-1})$ is the previous state posterior distribution at time step $k-1$, which is obtained based on the optimally selected sensor configuration $\mathbf{z}^{\star}_{k-1}$. Using the likelihood $p(\mathbf{y}_k|\mathbf{x}_k, \mathbf{z}_k)$ of measurement $\mathbf{y}_k$ that is obtained from the optimum sensor configuration $\mathbf{z}^{\star}_k$, the posterior distribution of the previous time step $p(\mathbf{x}_{k-1}|\mathbf{Y}^{\star}_{k-1}, \mathbf{Z}^{\star}_{k-1})$ is updated to obtain $p(\mathbf{x}_k|\mathbf{Y}_k, \mathbf{Z}_k)$. Taking the average of the posterior distribution $p(\mathbf{x}_k|\mathbf{Y}_k, \mathbf{Z}_k)$, the state estimator at time step k, $\hat{\mathbf{x}_k}$, is obtained. The performance metric in this case is the predicted RMSE J^p and is given by

$$\begin{aligned} J^p(\mathbf{z}_k) &\triangleq \left(E_{\mathbf{x}_k, \mathbf{y}_k}[(\mathbf{x}_k - \hat{\mathbf{x}}_k)(\mathbf{x}_k - \hat{\mathbf{x}}_k)^T]\right)^{1/2} \\ &= \left(\int\int (\mathbf{x}_k - \hat{\mathbf{x}}_k)(\mathbf{x}_k - \hat{\mathbf{x}}_k)^T p(\mathbf{y}_k|\mathbf{x}_k, \mathbf{z}_k) p(\mathbf{x}_k|\mathbf{y}_{k-1}, \mathbf{z}_{k-1}) d\mathbf{x}_k d\mathbf{y}_k\right)^{1/2} \end{aligned} \tag{4.4}$$

where

$$p(\mathbf{x}_k|\mathbf{y}_{k-1}, \mathbf{z}_{k-1}) = \int p(\mathbf{x}_k|\mathbf{x}_{k-1}) p(\mathbf{x}_{k-1}|\mathbf{Y}^{\star}_{k-1}, \mathbf{Z}^{\star}_{k-1}) d\mathbf{x}_{k-1} \tag{4.5}$$

The predicted RMSE J^p, in Equation (4.4) can be simplified by approximating it using

Monte Carlo integration

$$J^p(\mathbf{z}_k) \approx \left(\frac{1}{N} \sum_{i=1}^{N} \frac{1}{M} \sum_{\ell=1}^{M} (\mathbf{x}_k^i - \hat{\mathbf{x}}_k(\mathbf{y}_k^{\ell,i}))(\mathbf{x}_k^i - \hat{\mathbf{x}}_k(\mathbf{y}_k^{\ell,i}))^T \right)^{1/2} \tag{4.6}$$

For each sensor configuration $\mathbf{z}_k$, a corresponding predicted RMSE is calculated. In Equation 4.6, the first summation is for the number of state particles N and the second summation is for the number of measurement particles M, which are drawn based on each state particle $i = 1, ..., N$. Equation (4.6) shows the computational complexity of the predicted RMSE method. As the number of measurement and state particles increases, the cost increases as well. Considering the measurement equation of the dipole source model in Equation (3.2), each dipole has six unknown parameters: 3-D Cartesian coordinates of position and 3-D Cartesian coordinates of moment. Note that since the moment and position are non-linearly related in the measurement model, they can be separated in order to simplify the complexity of the problem even if we are interested in only estimating the position of the dipole source.

The sensor configuration that provides the minimum predicted RMSE value is the optimum one $\mathbf{z}_k^\star$ that will be used. The more the number of possible sensor configurations, the higher the calculation cost will be. The computational cost constraint of the predicted RMSE method results in a limitation in the number of sensor configurations. If the number of sensor configurations R is more than 10, this method cannot be used and there are other approximation methods that can solve this optimization problem based on the nature and the properties of the optimization problem. Some of those are branch and bound or convex relaxation approximations [31, 32]. The optimum sensor configuration $\mathbf{z}_k^\star$ can be obtained using a

$$\mathbf{z}_k^\star = \underset{\mathbf{z}_k}{\operatorname{argmin}} \, \mathbf{Tr}\left(J^p(\mathbf{z}_k)\right) \tag{4.7}$$

where $\mathbf{Tr}(.)$ represents the matrix trace and is minimized based on a constraint to limit the total power consumption to $\mathscr{P}$:

$$\sum_{m=1}^{M} z_{k,m} C_m \leq \mathscr{P}, \tag{4.8}$$

where C_m is the power consumption of the mth sensor. In order to solve the above problem, the particle filter algorithm is used two times. The second particle filter is used to estimate the $\hat{\mathbf{x}}_k(\mathbf{y}_k^{\ell,i})$ of the predicted RMSE equation (4.4), which will be used to choose the

optimum sensor configuration. The first particle filter is used to update the previous time step posterior distribution based on the measurements of the optimum sensor configuration. A block diagram of the dipole state estimation and sensor scheduling method is shown in Figure 4.1.

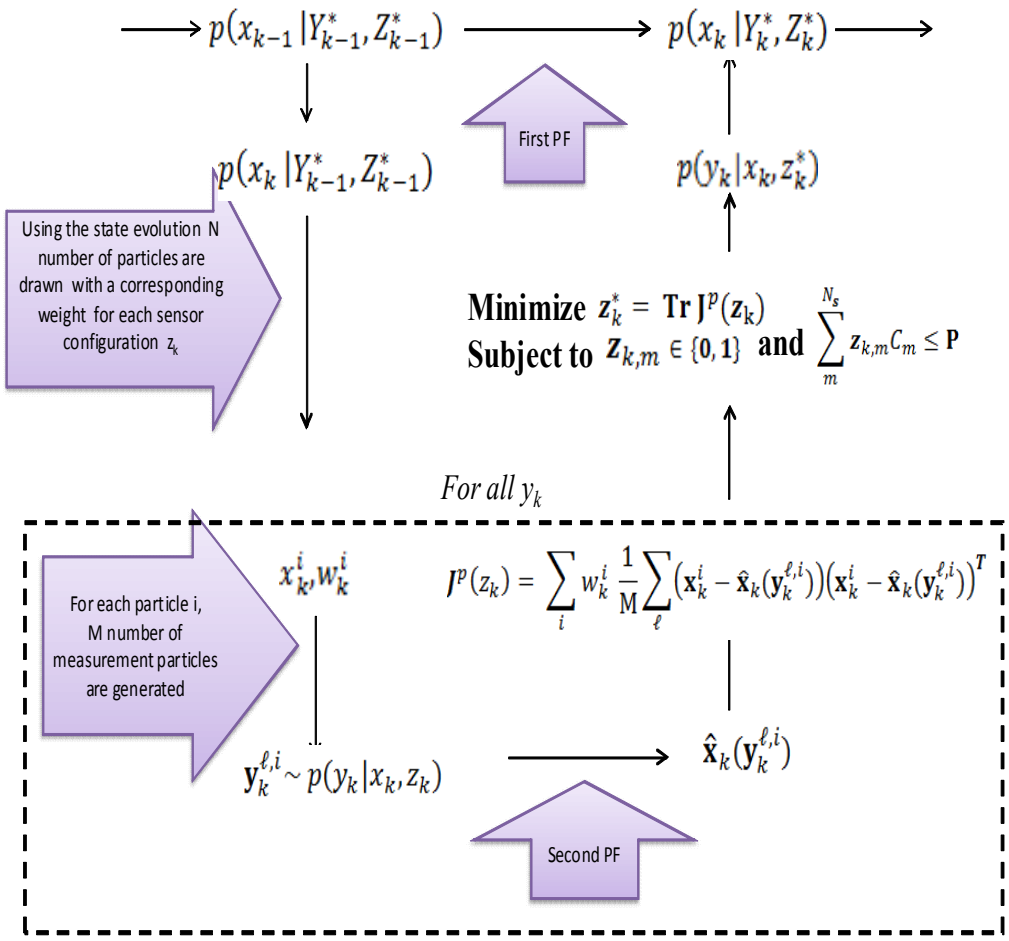

Figure 4.1: Sensor optimization diagram using the predicted RMSE. In this diagram the state estimation and sensor optimization methods are demonstrated.

4.2 Sensor scheduling with Maximum SNR

The second approach to find the optimum sensor configuration uses the distance between the previous state estimate $\mathbf{x}_{k-1}$ and the sensor locations as the performance metric. The fact that the variance of the dipole movement is not that large between each time step,

makes the use of the previous state estimate $\mathbf{x}_{k-1}$ a good estimation. Based on the leadfield for MEG in Equation (2.10) and EEG Equation in (2.13), the distance between the sensors and the dipole location is very important. As the distance between the dipole and electrode increases the primary current strength decreases. Therefore, this method maximizes the signal-to-noise ratio (SNR) of the measured sensor data. Suppose that at some time step k the parameters of the dipole sources $(\mathbf{r}_k, \mathbf{q}_k)$ are given and are fixed. From Equation (2.10) and (3.2), the SNR of the measurement from the mth sensor can be represented by

$$SNR_k^m = \frac{\sum_{j=1}^{N_d} \left(b_{k,j}(\mathbf{r}_m)\right)^2}{\sigma^2} \approx \sum_{j=1}^{N_d} \left(b_{k,j}(\mathbf{r}_m)\right)^2 \tag{4.9}$$

where $b_{k,j}(\mathbf{r}_m)$ is the magnetic field measured from the mth sensor, σ^2 is the variance of measurement noise and N_d is the number of dipole sources. From Equation (2.10), the magnetic field is a function of the distance $d_{k,m,j}$ between the mth sensor and jth dipole source. Figure 4.2 shows the relationship between the signal amplitude and the distance $d_{k,m,j}$. It can be observed that as the distance increases, the amplitude of the signal decreases, as well as the corresponding SNR. Since the MSE in estimation is expected to be lower with higher SNR measurements, using the sensors with smaller $d_{k,m,j}$ can provide better neural tracking performance.

In addition, in Chapter 2, it was indicated that artifacts are produced by movement charge from other surrounding tissues that do not contain valuable information about the areas of neuron activity. In general, artifacts' signals are everywhere in the head volume. The idea of this method is that the further the sensor is from the dipole source, the weaker the valuable information about the dipole source is. When the dipole is far from the sensor, the dipole signal is weak and the artifacts signals dominate. Therefore, taking those informations as a fact, it can be concluded that the sensors close to the dipole contain the most valuable information. This method is not proved mathematically but is a method based on the model and experimental observations. Moment is another significant information about the dipole, which is not consider in this method because it is believed that distance is in greater importance.

To begin this approach, the same assumption that the initial state $p(\mathbf{x}_0|\mathbf{Y}_0, \mathbf{Z}_0)$ is

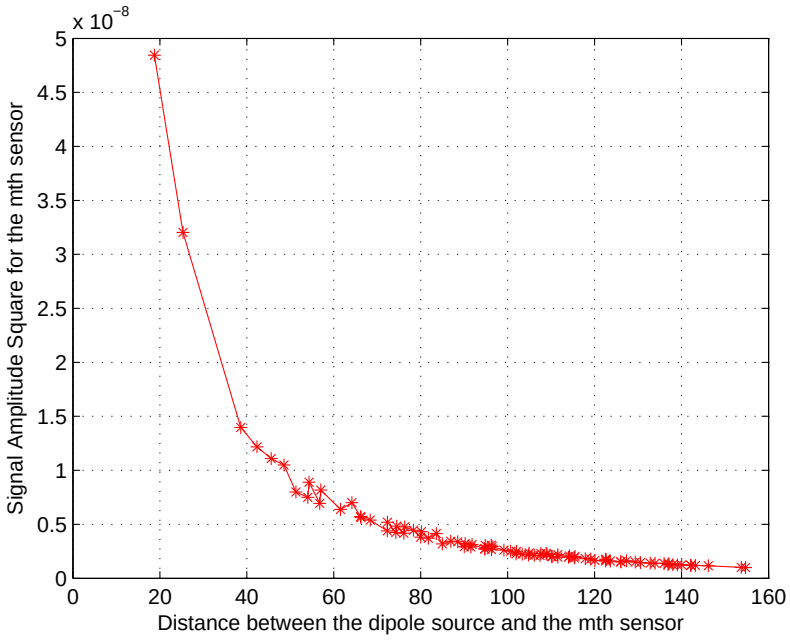

Figure 4.2: Amplitude of the sensor signal as a function of the distance between the sensor and the dipole source

known is required. Therefore, given the posterior distribution of the previous time step $p(\mathbf{x}_{k-1}|\mathbf{Y}^{\star}_{k-1},\mathbf{Z}^{\star}_{k-1})$, the distance between each dipole and each sensor is calculated. Assuming there are N_d number of dipoles and N_s number of sensors, the distance matrix can be calculated by using Euclidean distance equation which is given by

$$d_{j,m} = \sqrt{(x_j - x_m)^2 + (y_j - y_m)^2 + (z_j - z_m)^2} \tag{4.10}$$

where $m = 1,...,N_s$ is the variable for the number of sensors, $j = 1,...,N_d$ is the variable for the number of dipoles, and (x_j, y_j, z_j) and (x_m, y_m, z_m) are (x,y,z)-coordinates of the sensor location and the dipole location, respectively. For each dipole, the sensors are sorted in ascending sequence based on their distance from the dipole, $\tilde{d}_{k,m}$. The first $\mathfrak{s}$ sensors are selected to estimate the dipole states, where $\mathfrak{s}$ is the number of sensors to be used depending on power constraint in Equation 4.8. Using the above procedure the optimum sensor configuration $\mathbf{z}^{\star}$ can be calculated. Using the optimum sensor configuration $\mathbf{z}^{\star}$, a particle filter algorithm is used to obtain $p(\mathbf{x}_k|\mathbf{Y}_k,\mathbf{Z}^{\star}_k)$. Using the optimum sensor configuration $\mathbf{z}^{\star}_k$, the likelihood $p(\mathbf{y}_k|\mathbf{X}_k,\mathbf{Z}^{\star}_k)$ is calculated and used to update the posterior distribution of the previous time step $p(\mathbf{x}_{k-1}|\mathbf{Y}^{\star}_{k-1},\mathbf{Z}^{\star}_{k-1})$.

Table 4.1: Proposed Sensor scheduling with Maximum SNR Sample Algorithm

1. Calculate the predicted state of the dipole source $\tilde{\mathbf{x}}_k$ at time k using the particles $x_{k-1}^{(i)}$ and weights $w_{k-1}^{(i)}$ at time $k-1$ based on the state model

$$\tilde{\mathbf{x}}_k = \sum_{i=1}^{N} p_{x_{k-1}|x_k}(x_{k-1}^{(i)})\, w_{k-1}^{(i)},$$

   where N is the number of particles and $p_{x_{k-1}|x_k}(\cdot)$ is the state updating equation. Extract the predicted dipole location $\tilde{\mathbf{r}}_k$ from $\tilde{\mathbf{x}}_k$.

2. For each sensor m, calculate the distance between the sensor location $\mathbf{r}_m$ and the predicted dipole source location $\tilde{\mathbf{r}}_{k,j}$ as

$$\tilde{d}_{k,m} = ||\mathbf{r}_m - \tilde{\mathbf{r}}_{k,j,q}||, \quad m = 1,\ldots,M,$$

   where $||\cdot||$ denotes Euclidean distance.

3. Sort the sensors in increasing order of $\tilde{d}_{k,m}$. Choose the first $\mathfrak{s}$ sensors to estimate the dipole states, where $\mathfrak{s}$ is the number of sensors to be used depending on power constraint in Equation 4.8.

4. the scheduled sensor configuration $\mathbf{z}_k^*$ is then used to obtain the measurement $\mathbf{y}_k(\mathbf{z}_k^*)$ at time k and estimate the state $\hat{\mathbf{x}}_k$ using Particle Filter algorithm.

The advantage of the proposed method is the low computational cost since the optimization problem can be calculated fast. This is an advantage that makes that method easy to implement on hardware, which is the main purpose of this thesis. The next chapter will compare and analyse the results of both methods.

Chapter 5

SIMULATIONS AND RESULTS

For the simulations, all the algorithms and experiments were run on a MATLAB software. For all the experiments, MEG synthetic data were used and analysed based on the proposed optimization methods. For all the simulations, the number of dipoles are known, since the focus of this thesis is to localize the state of the dipole. Therefore, 2 dipoles are used and the number of sensors are 149 for each case. The data were created by inserting current dipoles into the sphere head model and calculating the resulting magnetic field using Equation (2.10) with Gaussian noise. This section presents all the results using both methods, using the predicted MSE and the distance between the sensors location and the previous state estimate as the performance metric. A number of figures and tables illustrate the performance of each method, introducing their advantages and disadvantages. A Monte Carlo simulation was run for each experiment in order to get a more reliable and good performance estimation. The first section analyses the performance of the predicted MSE method and the second section the distance between the sensors' previous state estimate.

5.1 Predicted RMSE results

The predicted RMSE method was introduced in the previous section and can be calculated based on the Equation (4.6). As explained in the previous section, the number of sensor combinations are 2^R, where R is the number of sensor configurations. Because of the high computational cost in the calculation procedure, we eliminate the first summation of equation over all the state particles N by taking their expected value. This approximation eliminates the computational cost by N times, which is the number of state particles. This made the algorithm much faster, since the number of particles that are used is 2500. This is an important approximation, which results in elimination of the high computational cost of this method. Even though this is an approximation, because of the small variance of the state particles, the performance of the estimation is not affected. Therefore, Equation (4.6)

is approximated to

$$
\begin{aligned}
J^p(\mathbf{z}_k) &\approx \left(\frac{1}{N} \sum_{i=1}^{N} \frac{1}{M} \sum_{\ell=1}^{M} (\mathbf{x}_k^i - \hat{\mathbf{x}}_k(\mathbf{y}_k^{\ell,i}))(\mathbf{x}_k^i - \hat{\mathbf{x}}_k(\mathbf{y}_k^{\ell,i}))^T \right)^{1/2} \\
&\approx \left(\frac{1}{M} \sum_{\ell=1}^{M} (\mathbf{x}_k - \hat{\mathbf{x}}_k(\mathbf{y}_k^{\ell}))(\mathbf{x}_k - \hat{\mathbf{x}}_k(\mathbf{y}_k^{\ell}))^T \right)^{1/2}
\end{aligned}
\tag{5.1}
$$

In the simulations, 50 measurement particles (M=50) are used. The number of sensors for the MEG data are 149, which makes it impossible to use this method since the number of combinations is too large (2^{149}). The maximum number of sensor configurations that can be used are usually 10, depending on the number of particles. In this case, the number of particles is large, which makes even 15 a large number of sensor configurations. Thus, the sensors are grouped in order to show and prove that the method can be used in order to find the optimum sensor configuration based on the predicted RMSE. In the experiment, we use total of 3 groups of fixed sensors, 2 groups of 50 and one of 49. The purpose of the experiment is to show that the predicted RMSE can actually predict the real RMSE and can be used as an optimization method for choosing the best sensor configuration. The results of the method could be even better if the sensors were distributed differently among the three groups. In each time step, two of the groups had to be activated and eliminate one. In this case, there are 3 possible combinations for each time step. For each time step, the combination that minimizes the predicted RMSE is the one that will be chosen as the optimum configuration.

In Figures 5.1 and 5.2, the predicted RMSE performance is compared to the actual RMSE for the first four time steps for each dipole. Furthermore, the actual RMSE using all sensors without any sensor scheduling is also demonstrated in the figures. Both figures show that the predicted RMSE can actually approximate the actual RMSE, which proves that the proposed method works. In addition, it can be observed that the use of sensor scheduling can achieve a good tracking performance compared with using all the sensors. Figure 5.3 demonstrates the overall performance of both dipoles, which makes the statement that the predicted RMSE method can actually predict the actual RMSE even stronger. It also shows that good tracking results can be achieved with sensor scheduling compared using all the sensors.

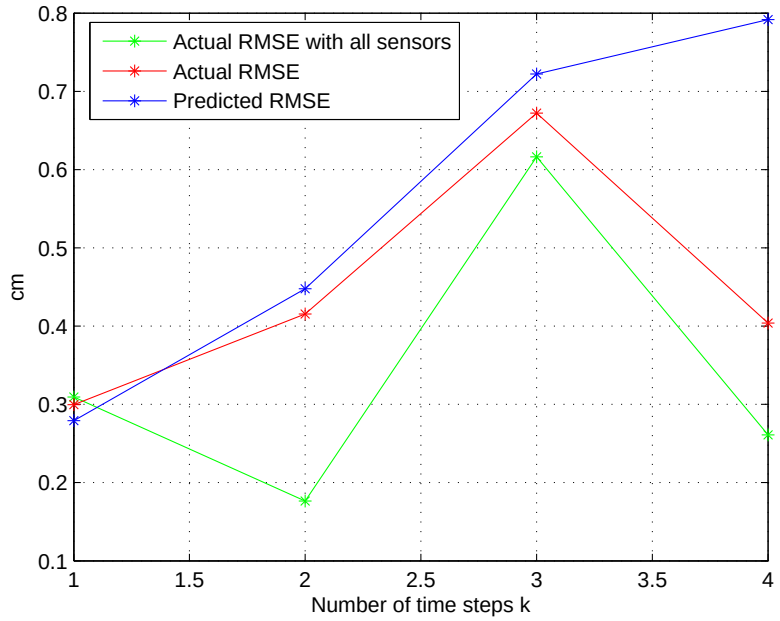

Figure 5.1: Actual RMSE Vs Predicted RMSE performance for the first 4 times steps of dipole 1.

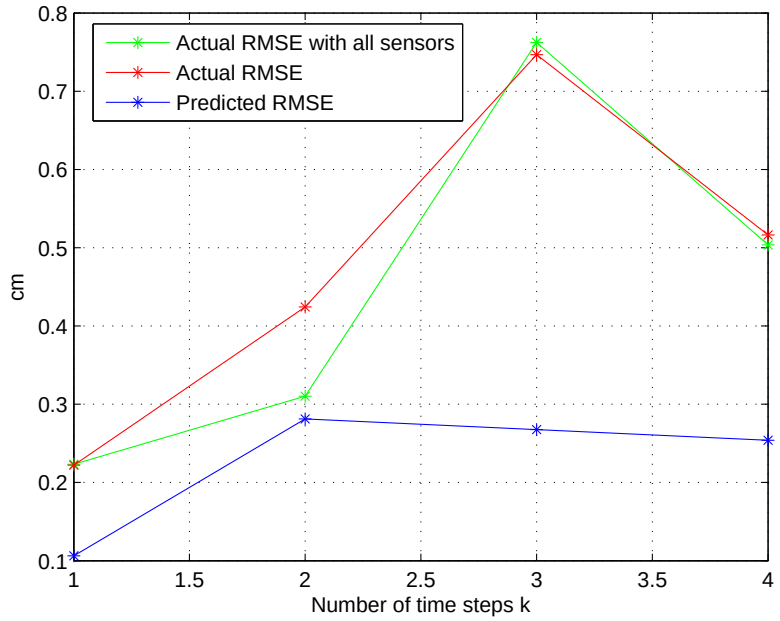

Figure 5.2: Actual RMSE Vs Predicted RMSE performance for the first 4 times steps of dipole 2.

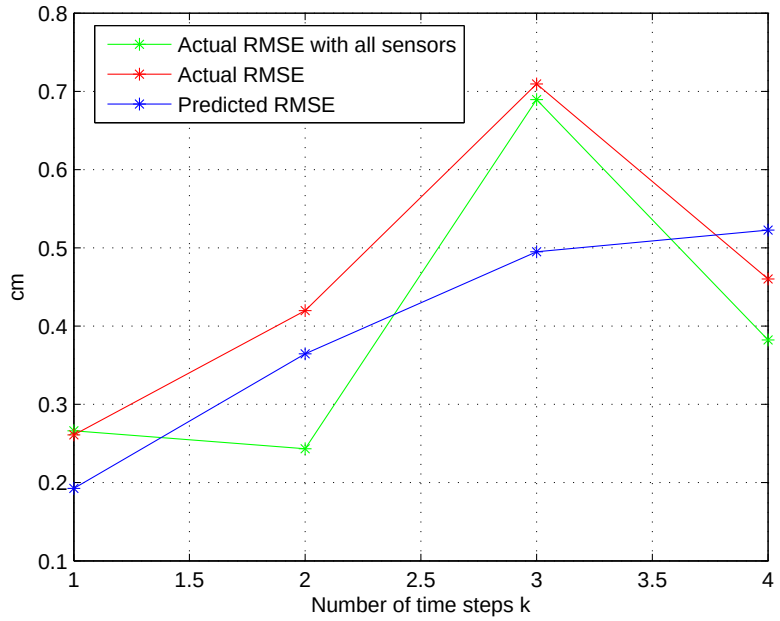

Figure 5.3: The total actual RMSE Vs Predicted RMSE performance for the first 4 times steps of both dipoles.

Table 5.1 shows the results of the actual RMSE and the predicted RMSE over all time steps. The results show a small difference between the actual RMSE and the predicted RMSE. Based on these results, the method proves to provide good tracking estimation performance. The performance of the method could be improved even more if we used a larger number of particles. However, this is a trade-off, since the larger the number of particles, the higher the computation cost is. Furthermore, this proves that the predicted RMSE can actually predict the actual RMSE. This is an important result that demonstrates that this method can be effectively used to provide the optimum sensor configuration that minimizes the actual RMSE.

Table 5.1: Predicted RMSE Method Results.

Number of Sensors	Predicted RMSE	RMSE
100	0.3937	0.4626

5.2 Sensor scheduling with Maximum SNR Results

For the second method, 3000 particles (N=3000) were used. Simulations were performed for different numbers of sensors s per dipole to show the performance of the proposed algo-

rithm. Monte Carlo simulations were performed for each study case to improve the reliability and accuracy of the results. Table 5.2 shows the results by using the proposed method for different values of activated sensors. The results are also plotted in Figure 5.7, where it shows that the method can provide a good tracking performance after approximately 30 sensors, 15 for each dipole. Based on the plot, as the number of sensors increases, the dipole tracking performance does not show a significant improvement. This shows that by reducing the sensor numbers, it is possible to get a good estimation of the location of the dipole. This also proves the importance of distance between the sensors location to the source localization. Moreover, the method shows that one of the dipole has better tracking performance than the other.

Table 5.2: Second Method Results for 5 Time Steps.

Number of Activated Sensors	RMSE Dipole 1 (cm)	RMSE Dipole 2 (cm)	RMSE Total (cm)
6	1.2487	1.2181	1.2334
10	0.9527	1.3854	1.1691
20	0.5347	0.7764	0.6556
30	0.4559	0.5602	0.5081
40	0.4361	0.6081	0.5221
50	0.4018	0.5968	0.4993
60	0.3667	0.5979	0.4823
70	0.4006	0.6008	0.5007
80	0.3811	0.5665	0.4738
100	0.3944	0.5664	0.4804

In order to present a more complete picture of the method, plots of the tracking performance in the case of a total of 60 sensors are shown below. The tracking performance of both dipoles are shown in 3-D plots. Calculating the distance between each dipole and the sensors, the first 30 closer to each dipole are selected. Figures 5.4 and 5.5 show a 3-D plot of dipole 1 and dipole 2 tracking performance for five time steps (k=5). The figures prove the effectiveness of the method. Figure 5.6 provides a more clear picture to the reader of how the method works. It shows the tracking performance of both dipoles and, at the same time, it shows the activated sensors for the last time step. From the figure, the reader can observe that the sensors that are close to the dipoles are activated and used for the solution of the inverse problem.

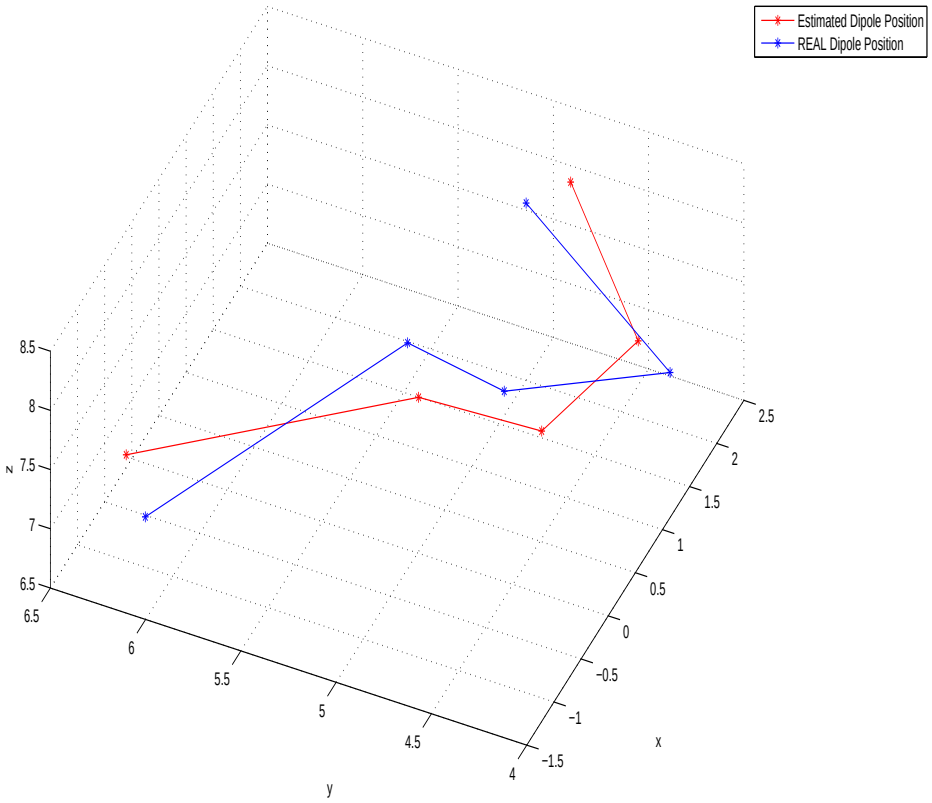

Figure 5.4: 3-D demonstration of the 2 dipole tracking performance using distance as performance metric. This figure shows dipole 1 tracking for 30 sensors per dipole.

5.3 Simulation Results for Sensor Scheduling Method

The previous sections shows the tracking performance of the sensor scheduling method, but it is important to demonstrate the meaning of sensor Scheduling. The main purpose of implementing sensor scheduling in the beginning of this thesis was to reduce the amount of data and reduce the power constraint. Table 5.3 shows the tracking performance and the data amount using all sensors and just 60 sensors using the distance method. Based on [33], for EEG/MEG test at each time step each sensor data word is 4 bytes. In Table 5.3 the RMSE performance for each dimension is demonstrated and the total data amount at the same time. Based on the results it can be observed that the performance of the distance method is almost the same with using all the sensors in x,z dimension and there is

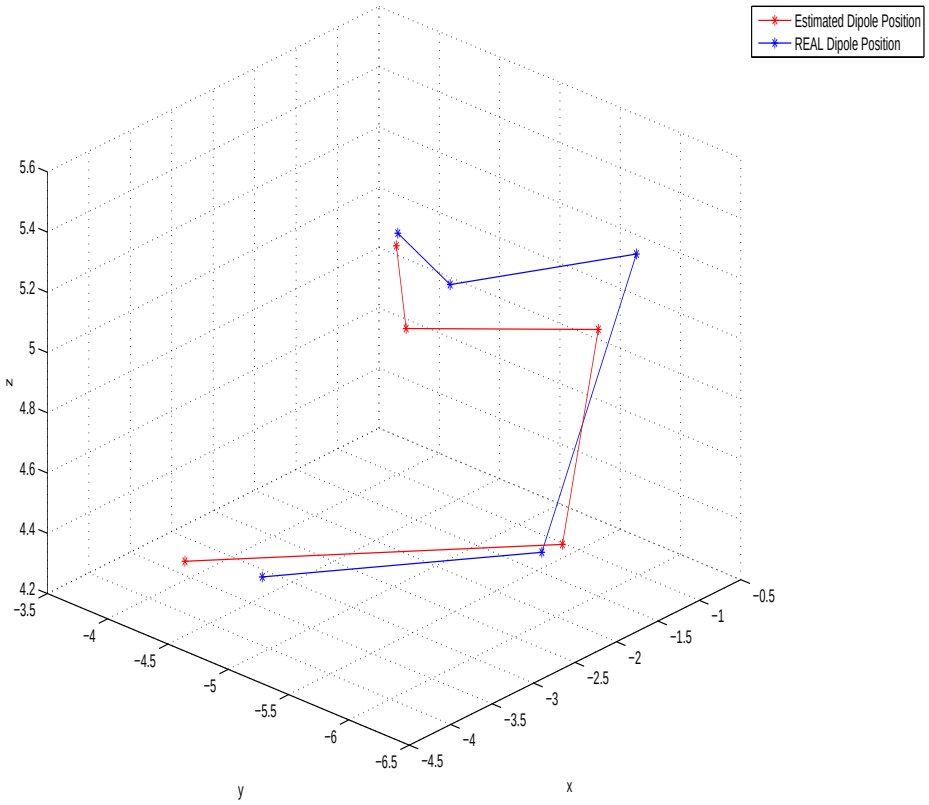

Figure 5.5: 3-D demonstration of the 2 dipole tracking performance using distance as performance metric. This figure shows dipole 2 tracking for 30 sensors per dipole.

a small gap between the y dimension. However, the amount of data generated by using all the sensors with significantly large. The goal of this thesis report it was to get reasonable good result and at the same time reduce the amount of data. To make this statement more realistic, it is important to see in a real EEG/MEG test for epilepsy how much data are generated for a ten minute period. For a typical epilepsy monitoring usually the sample rate is 2000 samples per second [33]. For a ten minute recording the data using all the sensors will be 715.2 MB and by just using 60 sensors will be 288MB. This shows how the sensor scheduling can significantly reduce the amount of data and at the same time get reasonable good dipole estimation performance. In addition, the power consumption of one wireless EEG sensor is on the order of 10 mW [34, 35]. For a total of 60 sensors the total power consumption will be 600mW compared to 1490mW using all the sensors.

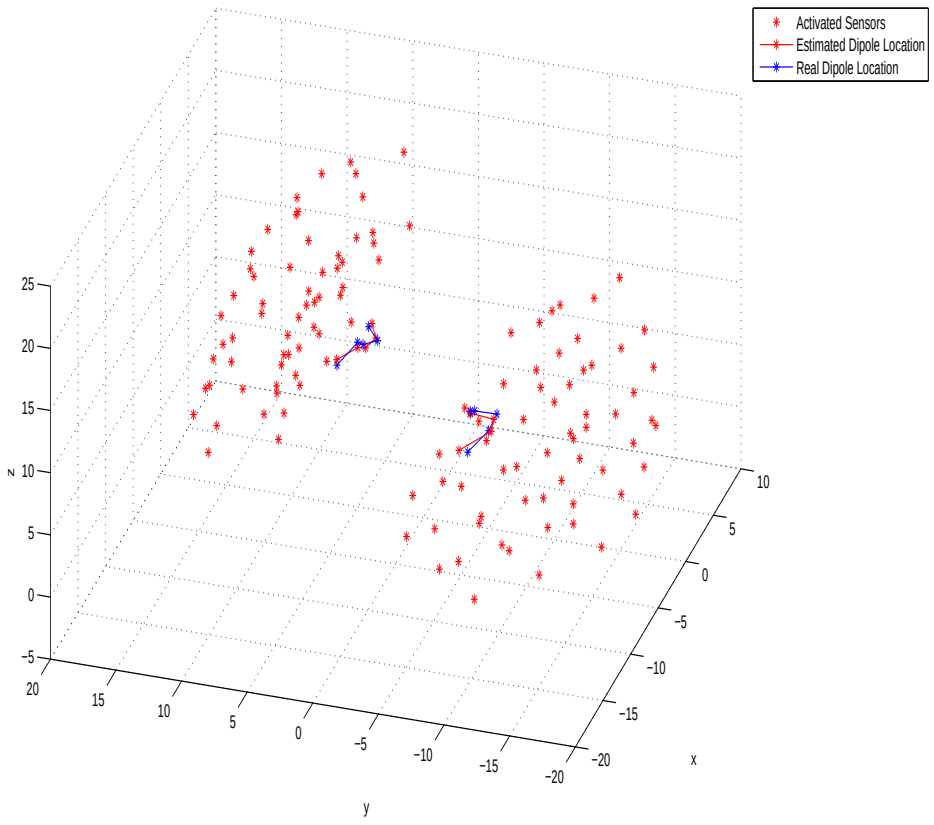

Figure 5.6: 3-D demonstration of the 2 dipole tracking performance using distance as performance metric. This figure shows both dipole tracking performance for 30 sensors per dipole and the activated sensors for the last time step.

Table 5.3: Simulation results demonstrating the data amount for each time step assuming that each sensor data word is 4 bytes per time step.

Number of Activated Sensors	RMSE x (cm)	RMSE y (cm)	RMSE z (cm)	Data stored per time step (byte)	Wireless power consumption (mW)
60 Sensors with Maximum SNR method	0.2998	0.2446	0.1674	240	600
Using all 149 sensors	0.2991	0.2286	0.1656	596	1490

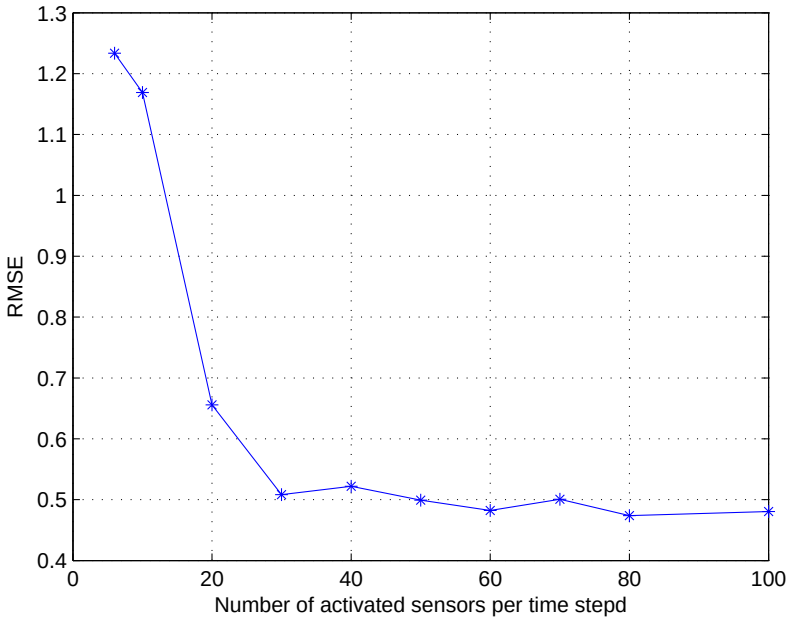

Figure 5.7: Actual RMSE with respect to the number of sensors activated per time step k.

Chapter 6

CONCLUSION

The neural system activity is a big area of study that can diagnose the existence and the cause of brain disorders. The number of people that suffer from brain disorders has increased dramatically and the study of those disorders is much needed. One of the most known brain disorders is Epilepsy, which is characterised by transient and unexpected electrical disturbances of the brain. The high rates of people who suffer from epilepsy increases the need of further studying it. This thesis focused in the source localization of those abnormal disturbances of the brain. Using brain activity monitoring data coming from MEG and EEG tests, doctors can diagnose the different brain disorders. Both tests are performed by collecting data from multiple sensors (electrodes), which are attached on a patient's head. The last couple of years a new technique known as Ambulatory EEG is used for improving the quality and accuracy of brain disorders. According to this method, the EEG system is portable and can be used in the natural environment of the patient, which might be one of the reasons that cause the seizure disorder. The disadvantage of the current AEEG is the inconvenience to the patient due to the electrode's wires and the weight of the system. To overcome the disadvantages of the current AEEG, a new method called wearable EEG is proposed in order to replace the heavy and inconvenient AEEG. The proposed devices are smaller, they can be attached on the scalp of the patient, and can record EEG for longer periods of time [4–6]. The proposed method will provide long term monitoring of brain activity, which is important for some brain disorders that require long term monitoring in order to observe higher likelihood of seizures. There are several obstacles that researchers need to overcome in order to make AEEG a reliable and beneficial device for studying brain disorders. One of the constraints of the new device is the large amount of data for storage and transmission that long period recordings require [4]. According to [4], the amount of data for the 24 period recording is estimated to be 1GB. This results in the power constrain issue, since in order to obtain long term recordings, large amount of power are needed. This thesis paper examines the power constraint issue and provides two sensor scheduling algorithms that reduce the number of sensors that are activated in each time step. Less sensors

will result in less data to store and transmit.

The first proposed algorithm uses the predicted RMSE as the performance metric for optimum sensor configuration selection. This method proved that it can predict the optimum sensor configuration and can improve the accuracy performance of the dipole estimation. Its main disadvantage is the high computational cost, which makes it unrealistic for hardware implementation. Even though the calculation cost is reduced by N times using an approximation, it cannot be implemented for large amount of sensor configurations. The second proposed algorithm is a heuristic method based on the distance between the sensors and the previous time step state estimate. Since the movement variance of the dipole at each time step is not significantly large, the results prove that this is a good estimation. The plot of RMSE with respect to the number of activated sensors shows that after approximately 30 sensors (15 for each dipole), the RMSE are stable and there is no significant improvement in the error performance. This demonstrates that by reducing the sensor number, it is possible to get a good state estimate of the location of the dipole. This also proves the importance of distance between the sensors location to the source localization. The advantage of the second proposed method is the low computational cost, which makes it ideal for hardware implementation. Although the first method provides better estimation results with lower RMSE, it has the disadvantage high computational cost. Therefore, there is a trade off between the two methods.

Overall, both methods demonstrate that good estimation results can be achieved with less sensors. This is important because reducing the number of sensors at each time step results in significantly reducing the amount of data that are transmitted and stored each time step. This solves the power constraint issue that was the main motivation of this thesis. In addition, in real data, fewer sensors will result in less external (hardware noise) and internal artifacts, which will improve the quality of measurements. Artifacts, which are basically the measurement noise in this case, is another big area of study and a lot of research is conducted on how to decompose the dipole signal from artifacts. Implementation of the proposed method can possibly reduce the EEG/MEG artifacts because the idea of sensor scheduling is to select the sensors that provide the best measurements. Rejecting

the sensors with bad measurement could result in reducing the amount of artifacts in the recorded data. This can be part of future work and study, since this thesis did not focus on the artifacts removal.

Neural signal activity is a big area of research and a lot of future work can be done to solve the power constraint issue, including improving algorithm development or hardware development. In real world implementations, algorithms should provide good estimation performance and low computational cost. As the number of sensors increase, the computational cost increases. Some approximation methods based on convexity of the system have been proved to provide results with low computational cost and good estimation performance. Therefore, proving that the optimization problem is a convex function, branch and bound methods or any other convex relaxation based methods can be used to solve the aforementioned problem [31, 32].

REFERENCES

[1] S. Baillet, "MEG/EEG principles and instrumentation," 2010, accessed April 12, 2012. [Online]. Available: http://www.canada-meg-consortium.org/EN/MegBaillet2

[2] J. Malmivuo and R. Plonsey, *Bioelectromagnetism: Principles and Applications of Bioelectric and Biomagnetic Fields*. OXFORD UNIVERSITY PRESS, 1995.

[3] S. Baillet, J. C. Mosher, and R. M. Leahy, "Electromagnetic brain mapping," *IEEE Signal Processing Magazine*, vol. 18, no. 6, pp. 14–30, 2001.

[4] A. J. Casson, S. Smith, J. S. Duncan, and E. Rodriguez-Villegas, "Wearable EEG: what is it, why is it needed and what does it entail?" in *Proceeding of the 30th Annual International Conference of the IEEE Engineering in Medicine and Biology Society*, 2008, pp. 5867–5870.

[5] A. J. Casson and E. Rodriguez-Villegas, "Data reduction techniques to facilitate wireless and long term AEEG epilepsy monitoring," in *Proceeding of the 3rd International IEEE/EMBS Conference on Neural Engineering*, 2007, pp. 298–301.

[6] D. Yates, E. Lopez-Morillo, R. G. Carvajal, J. Ramirez-Angulo, and E. Rodriguez-Villegas, "A low-voltage low-power front-end for wearable EEG systems," in *Proceeding of the 29th Annual International Conference of the IEEE Engineering in Medicine and Biology Society*, 2007, pp. 5282–5285.

[7] J. Gotman, "Automatic detection of seizures and spikes," *Clinical Neurophysiology*, vol. 16, pp. 130–140, 1999.

[8] A. J. Casson, D. C. Yates, S. Patel, and E. Rodriguez-Villegas, "Algorithm for AEEG data selection leading to wireless and long term epilepsy monitoring," in *Proceeding of the 29th Annual International Conference of the IEEE Engineering in Medicine and Biology Society*, 2007, pp. 2456–2459.

[9] G. Antoniol and P. Tonella, "EEG data compression techniques," *IEEE Engineering in Medicine and Biology Society*, vol. 44, no. 2, pp. 105–114, 1997.

[10] J. Cardenas-Barrera, J. Lorenzo-Ginori, and E. Rodriguez-Valdivia, "A wavelet-packets based algorithm for EEG signal compression," *Medical Informatics & The Internet in Medicine*, vol. 29, pp. 15–27, 2004.

[11] L. Miao, J. J. Zhang, C. Chakrabarti, A. Papandreou-Suppappola, and N. Kovvali, "Real-time closed-loop tracking of an unknown number of neural sources using probability hypothesis density particle filtering," in *IEEE Workshop Signal Processing Systems*, 2011, pp. 367–372.

[12] L. Miao, J. J. Zhang, C. Chakrabarti, and A. Papandreou-Suppappola, "A new parallel implementation for particle filters and its application to adaptive waveform design," in *Proceeding of the IEEE Workshop on Signal Processing Systems*, 2010, pp. 19–24.

[13] M. T. Wolf and J. W. Burdick, "Multiple hypothesis tracking using clustered measurements," in *IEEE International Conference on Robotics and Automation*, 2009, pp. 3955–3961.

[14] W. Zhou, N. Kovvali, A. Papandreou-Suppappola, and A. Chattopadhyay, "Sensor optimization for progressive damage diagnosis in complex structures," *Proceedings of SPIE*, vol. 7650, 2010.

[15] A. S. Chhetri, D. Morrell, and A. Papandreou-Suppappola, "On the use of binary programming for sensor scheduling," *IEEE Transactions on Signal Processing*, vol. 55, no. 6, pp. 2826 – 2839, 2007.

[16] J. C. Mosher, R. M. Leahy, and P. S. Lewis, "EEG and MEG: forward solutions for inverse methods," *IEEE Transactions on Biomedical Engineering*, vol. 46, no. 3, pp. 245–259, 1999.

[17] J. J. Ermer, J. C. Mosher, S. Baillet, and R. M. Leahy, "Rapidly recomputable EEG forward models for realistic head shapes," *Physics in Medicine and Biology*, vol. 46, pp. 1265–1281, 2001.

[18] P. Berg and M. Scherg, "A fast method for forward computation of multiple-shell spherical head models," *Electroencephalography and Clinical Neurophysiology*, vol. 90, pp. 58–64, 1994.

[19] Z. Zhang, "A fast method to compute surface potentials genrated by dipoles within multilayer anisotropic spheres," *Physics in Medicine and Biology*, vol. 40, pp. 335–349, 1995.

[20] T. Liu and D. Yao, "Removal of the ocular artifacts from EEG data using a cascaded spatio-temporal processing," *Elsevvier Ireland*, vol. 83, pp. 95–103, 2006.

[21] N. Ye, X. Wang, and Y. Sun, "Independent component analysis and time-frequency method for noisy EEG signal analysis," in *Proceeding of the 8th International Conference on Signal Processing*, vol. 4, 2006.

[22] M. A. Kladosa, C. Papadelisb, C. Braunb, and P. D. Bamidis, "REG-ICA: A hybrid methodology combining blind source separation and regression techniques for the rejection of ocular artifacts," *Biomedical Signal Processing and Control*, vol. 6, pp. 291–300, 2011.

[23] I. Navarro, B. Hubais, and F. Sepulveda, "A comparison of time, frequency and ICA based features and five classifiers for wrist movement classification in EEG signals," in *Proceeding of the 27th Annual International Conference of the Engineering in Medicine and Biology Society*, 2005, pp. 2118–2121.

[24] J. Valer, T. Daisuke, and D. Ippeita, "10/20, 10/10, and 10/5 systems revisited: Their validity as relative head-surface-based positioning systems," *Neuroimage*, vol. 34, pp. 1600–1611, 2007.

[25] D. M. Tucker, "Spatial sampling of head electrical fields: the geodesic sensor net," *Electroencephalography and clinical Neurophysiology*, vol. 87, pp. 154–163, 1993.

[26] H. H. Jasper, "The ten-twenty electrode system of the international federation," *Electroencephalography and Clinical Neurophysiology*, vol. 10, pp. 367–380, 1958.

[27] B. Ristic, S. Arulampalam, and N. Gordon, *Beyond the Kalman Filter: Particle Filters for Tracking Applications*. Artech, 2004.

[28] T. M. Arinbjarnarson, "Bayesian approach to the ill-posed eeg inverse problem," Ph.D. dissertation, Technical University of Denmark, 2007.

[29] P. Maybeck, *Stochastic Models, Estimation, and Control*. Academic Press, Inc, 1979.

[30] L. Miao, J. J. Zhang, C. Chakrabarti, and A. Papandreou-Suppappola, "Multiple sensor sequential tracking of neural activity: Algorithm and FPGA implementation," in *Asilomar Confererence on Signals, Systems and Computers*, 2010, pp. 369–373.

[31] S. Joshi and S. Boyd, "Sensor selection via convex optimization," *IEEE Transactions on Signal Processing*, vol. 57, no. 2, pp. 451–462, 2009.

[32] S. Boyd and L. Vandenberghe, *Convex Optimization*. Cambridge University Press, 2010.

[33] J. Vrba and S. E. Robinson, "Signal processing in magnetoencephalography," *Methods*, vol. 25, pp. 249–271, 2001.

[34] N. Verma, A. Shoeb, J. Bohorquez, J. Dawson, J. Guttag, and A. P. Chandrakasan, "A micro-power EEG acquisition soc with integrated feature extraction processor for a chronic seizure detection system," *IEEE Journal of Solid-State Circuits*, vol. 45, pp. 804–816, 2010.

[35] Y. M. Chi, S. R. Deiss, and G. Cauwenberghs, "Non-contact low power EEG/ECG electrode for high density wearable biopotential sensor networks," *Wearable and Implantable Body Sensor Networks*, pp. 246 – 250, 2009.